Journal of Volcanology and Geothermal Research 373 (2019) 1–22

Contents lists available at ScienceDirect

Journal of Volcanology and Geothermal Research

journal homepage: www.elsevier.com/locate/jvolgeores

Evolution in magma storage conditions beneath Kick-'em-Jenny and Kick-'em-Jack submarine volcanoes, Lesser Antilles arc

Michal Camejo-Harry [a,b,*], Elena Melekhova [b], Jon Blundy [b], Richard Robertson [a]

[a] The University of the West Indies Seismic Research Centre, St. Augustine, Trinidad and Tobago
[b] School of Earth Sciences, University of Bristol, Wills Memorial Building, Bristol BS8 1RJ, UK

ARTICLE INFO

Article history:
Received 29 October 2018
Received in revised form 23 January 2019
Accepted 26 January 2019
Available online 30 January 2019

Keywords:
Kick-'em-Jenny
Lesser Antilles
Submarine volcanism
Melt inclusions
Hornblende

ABSTRACT

Kick-'em-Jenny and Kick-'em-Jack are two submarine volcanoes located in the southern Lesser Antilles arc. We present data on the temporal and spatial compositional variations in lavas and melt inclusions from Kick-'em-Jenny and four lavas from Kick-'em-Jack. Analyses of crater samples from Kick-'em-Jenny show an evolution in magma compositions between 1972 and 2013/14. Rock types have progressed from predominantly basalts in 1972 to basaltic andesites in 2013/14, while melt inclusions have also become more silicic over time, ranging basaltic to andesitic in 1972 and basaltic andesite to dacitic in 2013/14. Hornblende-phyric basalts are unusually rich in MgO (≤13 wt%) and Ni (≤230 ppm) and contain rare olivine phenocryst cores of $Fo_{90–92}$, suggestive of a primitive character. Other phenocryst phases include spinel, clinopyroxene and plagioclase. Conversely, 2013/14 landslide deposit samples contain orthopyroxene as an additional phenocryst phase and are distinct from crater deposits in terms of phenocryst and bulk rock chemistry. We propose that 1972 and 2013/14 crater deposits sample Kick-'em-Jenny's current edifice, whereas 2013/14 landslide deposits likely represent "proto Kick-'em-Jenny" (an edifice existing pre 43.5 kyr BP). Geochemical data for Kick-'em-Jack support the notion that it is part of the same volcanic complex as Kick-'em-Jenny and probably represents part of the now collapsed proto Kick-'em-Jenny.

Low eruption temperatures (~1000 °C), estimated from geothermometry, coupled with whole-rock magma chemistry suggest an origin of the most mafic lavas of Kick-'em-Jenny by dehydration melting of hornblende-peridotite just below the Moho. Subsequent injection of these cool, oxidised, wet primitive basalts into the deep crust was accompanied early fractionation of hornblende-dominated assemblages. Large, zoned hornblende phenocrysts track rapid ascent of magmas through the crust along a trajectory sub-parallel to the hornblende liquidus curve. Melt inclusion data provide clear evidence of volatile-rich (≤5 wt% H_2O and <3200 ppm CO_2) pre-eruptive magma storage 7–12 km below Kick-'em-Jenny. This new understanding of the architecture of Kick-'em-Jenny's sub-volcanic system will be useful for interpreting future seismic signals and mitigating volcanic hazards.

1. Introduction

Underwater eruptions are the most common type on Earth, yet little is known about submarine volcanoes compared to their subaerial counterparts. This is largely due to the difficulty in making direct observations of underwater eruptions. Monitoring of submarine volcanoes is typically limited to land-based seismic networks and reconnaissance ship surveys. A key drawback to our understanding of both submarine and subaerial volcanoes is our inability to directly observe the configuration of magma reservoirs and the processes operating beneath volcanoes. Technological advancements have made the imaging of sub-volcanic systems possible through geophysical surveys, however the acquisition of such measurements is often contingent on access to equipment and resources that are not often readily available. Petrological and geochemical observations of volcanic rock samples provide an alternate means of retrospective imaging of crustal reservoirs as crystals and their entrapped melts record the changing chemical and thermal conditions occurring within reservoirs before eruption (Cooper, 2017).

Here, we focus on lava samples from two submarine volcanoes in the Lesser Antilles arc: Kick-'em-Jenny and Kick-'em-Jack. We integrate new petrological and geochemical data for lavas and phenocryst-hosted melt inclusions with seismic data to constrain the vertical extent

* Corresponding author at: The University of the West Indies Seismic Research Centre, St. Augustine, Trinidad and Tobago.
E-mail address: michal.camejo@uwiseismic.com (M. Camejo-Harry).

https://doi.org/10.1016/j.jvolgeores.2019.01.023
0377-0273/

of sub-volcanic magmatic systems and pre-eruptive magma storage conditions with implications for monitoring and hazard assessment.

1.1. Volcanic activity and previous research

Kick-'em-Jenny and Kick-'em-Jack mark the southernmost culmination of volcanism in the Grenadines archipelago of the Lesser Antilles arc (Fig. 1), a 750 km-long, intra-oceanic island chain resulting from the slow westward subduction (~2 cm/yr) of the North and South American plates beneath the Caribbean plate. Magma production rates for this arc are comparatively low (Wadge, 1984), with only nine of twenty one potentially active volcanoes displaying historical eruptive activity (Camejo and Robertson, 2013).

1.1.1. Kick-'em-Jenny

Located 8 km north of Grenada, Kick-'em-Jenny is the only known active submarine volcano in the Lesser Antilles (Lindsay and Shepherd, 2005). Its asymmetric cone, 197 m below sea level, is the result of irregular periods of constructive edifice building during eruptive episodes interspersed with mass wasting (Allen et al., 2018). Although the volcano's existence first became known following felt explosions related to an eruption in 1939 (Devas and MacAdam-Sherwin, 1939), monitoring by the University of the West Indies, Seismic Research Centre (UWI-SRC) only began when this agency was established in 1953. Fourteen eruptions have been documented (Table 1), detected by human observation and/or seismometer recordings of T-phase episodes (Lindsay and Shepherd, 2005). The most recent detected eruption was in 2017, making it the most historically active volcano of the entire arc.

Kick-'em-Jenny's proclivity for edifice instability is evident from its morphology and landslide deposits. The current cone lies within a horseshoe-shaped collapse scar (formed at least 43.5 kyr BP based on radiocarbon dating, Dondin et al. (2017)), which is open to the west (Lindsay et al., 2005), with numerous associated landslide deposit sequences downslope (Fig. 1). This horseshoe feature is thought to represent the remains of the near-total collapse of an ancestral "proto Kick-'em-Jenny" edifice from which the current edifice now emerges. The proto edifice is modelled to have stood above sea-level before its subsequent failure (Dondin et al., 2012). Recent evaluation of bathymetric data indicates that over the past thirty years, cone-building episodes

Table 1
Historical eruptions at Kick-'em-Jenny volcano.
(Modified after Lindsay and Shepherd (2005).)

Eruption date	Evidence for eruption		
	T-phase signal	Felt earthquakes	Surface manifestations: water disturbances, ejected material, gases
July 24, 1939	–	✓	✓
Oct. 5–6, 1943	✓	✓	–
Oct. 30, 1953	✓	✓	–
Oct. 24, 1965	✓	✓	–
May 5–7, 1966	✓	–	–
Aug. 3–6, 1966	✓	✓	–
July 5, 1972	✓	–	–
Sept. 6, 1974	✓	–	✓
Jan. 14, 1977	✓	–	–
Dec. 29–30, 1988	–	✓	✓
March 26 to April 5, 1990	✓	✓	–
Dec. 4–6, 2001	✓	✓	–
July 23–24, 2015	✓	✓	–
April 29, 2017	✓	✓	–

Data taken from Latchman et al. (2017), Robertson et al. (2015) and Lindsay and Shepherd (2005).

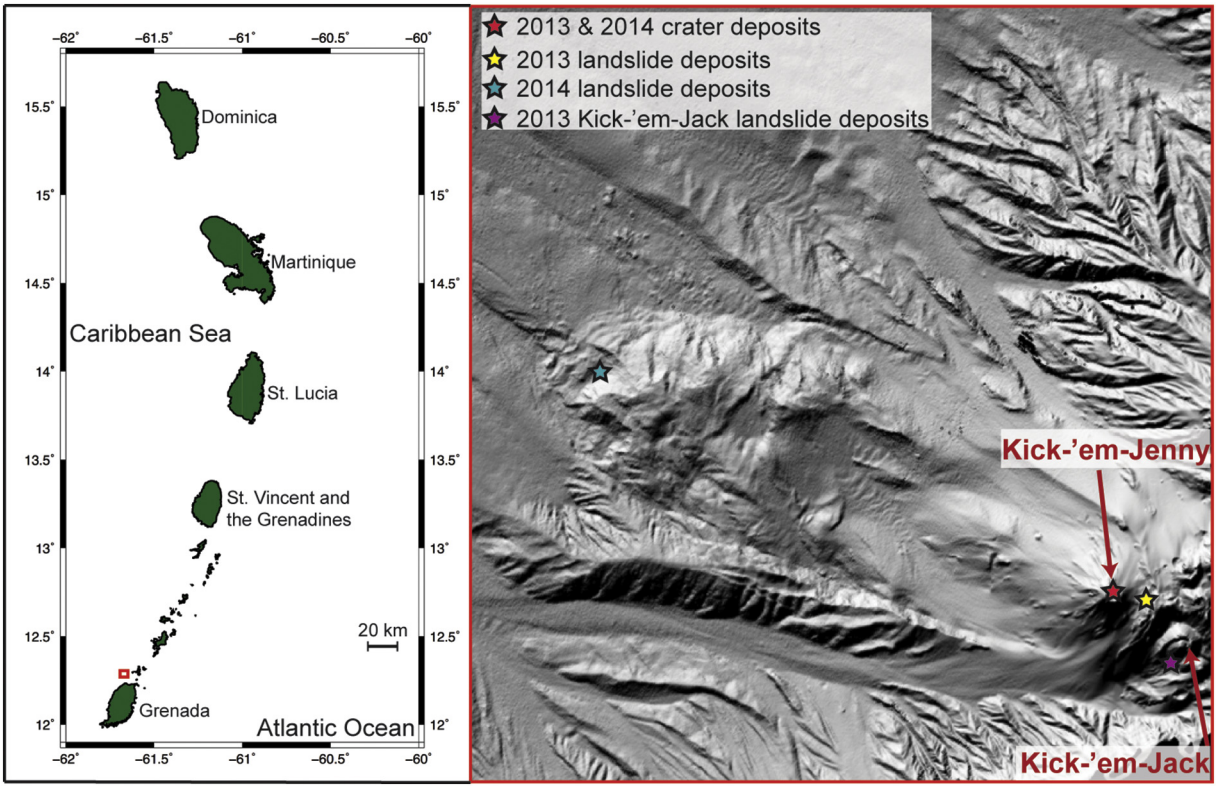

Fig. 1. Map showing location of Kick-'em-Jenny and Kick-'em-Jack volcanoes. Bathymetry is derived from multibeam data collected on the E/V Nautilus NA039 cruise in 2013. Inset map shows location of these volcanoes (red rectangle) in relation to the southern half of the Lesser Antilles arc. Stars denote locations of samples collected from Kick-'em-Jenny and Kick-'em-Jack in 2013 and 2014. 1972 samples (not shown) are reported to have been collected from various parts of the cone and crater (Sigurdsson and Shepherd, 1974).

have been infrequent with significantly more material being shed from the edifice during debris avalanche events triggered by seismicity or explosive eruptions (Allen et al., 2018). Although submarine landslides can be a key contributor to tsunami generation, the scientific consensus remains that the volcano's current vent height is insufficient to generate a tsunami (Allen et al., 2018; Lindsay et al., 2005). Of more immediate concern are the direct hazards associated with the volcano, such as ballistic ejecta, water disturbances and lowered water-column density due to degassing (Lindsay et al., 2005).

Kick-'em-Jenny erupts both explosively and effusively. The deciding mechanism for which style of activity will characterize a given eruption remains unclear. Estimated H_2O contents of pre-eruptive magmas at Kick-'em-Jenny suggest that they are enriched in volatiles while stored at magma reservoir depths. Devine and Sigurdsson (1995) alluded to the amount of pre-eruptive degassing of volatiles from saturated magma determining the style of activity: efficient magma degassing produces effusive eruptions while significant retention of dissolved volatiles generates explosive eruptions. The extent to which magma can degas depends ultimately on the rate of magma ascent and the permeability of the plumbing system. Currently, the former mechanism remains poorly understood, but the latter has been tackled by deformation experiments on rock samples collected from Kick-'em-Jenny. Fractures created by brittle deformation of edifice rocks promote efficient outgassing, favouring lava dome formation on this volcano (Dondin et al., 2017). Gas escape though interconnected bubble networks within magmas can also produce extrusive activity (Melnik et al., 2005). However, triggering of explosive behaviour by rapid magma ascent, irrespective of edifice permeability (Dondin et al., 2017), as well as magma interaction with external water (Devine and Sigurdsson, 1995) cannot be ruled out.

Petrological studies on Kick-'em-Jenny have been scarce due to the availability of rock samples. The earliest petrological studies were of rocks collected on the Royal Navy oceanographic research vessel *H.M.S. Hecla* in May 1972 (Devine and Sigurdsson, 1995; Sigurdsson and Shepherd, 1974). The principal rock types are scoriaceous, porphyritic basalt and minor basaltic andesites and andesites with abundant hornblende phenocrysts. There are few examples globally of hornblende bearing basalts e.g. Rhon, Germany (Mayer et al., 2013); Cerro La Pilita, Western Mexico (Luhr and Carmichael, 1985); Mount Lamington, Papua New Guinea (Arculus et al., 1983); Bogoslof, Alaska (Arculus et al., 1977). The presence of hornblende as a basaltic phenocryst has prompted interest in the water content of primary magmas in island arcs and the role of hornblende in crustal differentiation (Devine and Sigurdsson, 1995). Volcanic sediment collected on a 2003 *R/V Ronald H. Brown* cruise from areas of hydrothermal activity has also been studied in the context of hydrothermal alteration (Olsen, 2011).

1.1.2. Kick-'em-Jack

Kick-'em-Jack, located 3 km east of Kick-'em-Jenny (Fig. 1), was first discovered during the scientific cruise by the *R/V Ronald H. Brown* in 2003 (Carey et al., 2014; Lindsay and Shepherd, 2005). Bathymetric mapping revealed that Kick-'em-Jack, along with four other submarine craters and domes, lies towards the east of Kick-'em-Jenny. These features are inferred to be older than Kick-'em-Jenny and no longer active (Lindsay and Shepherd, 2005), however some low-level hydrothermal activity was observed between Kick-'em-Jenny and Kick-'em-Jack in 2003 (Carey et al., 2014). Kick-'em-Jack is described as similar in size to Kick-'em-Jenny with its own horseshoe-shaped crater enclosing a dome (Carey et al., 2014). The close association of Kick-'em-Jack with Kick 'em Jenny suggests that they may both belong to the same volcanic complex including the now-collapsed proto Kick-'em-Jenny volcano (Lindsay and Shepherd, 2005). The first and only petrological description to date of deposits from Kick-'em-Jack was provided by Christopher et al. (2016) on rock samples collected on the NA039 research cruise on the *E/V Nautilus* in 2013. Samples analysed were basaltic andesites and andesites containing up to 35 vol% phenocrysts of plagioclase, hornblende and minor clinopyroxene.

2. Methods

2.1. Sampling

For this study, lava samples were obtained from the Exploration Vessel *E/V Nautilus* cruises NA039 during 1–18 November 2013 and NA054 during September 21 to October 9, 2014 using a remotely operated vehicle. From the 2013 cruise, we analysed eleven samples from Kick-'em-Jenny's crater and three from a nearby debris avalanche deposit (Fig. 1). A further four samples were analysed from debris avalanche deposits associated with Kick-'em-Jack. These represent a subset of the first documented collection of samples from Kick-'em-Jack volcano. From the 2014 cruise, we analysed four samples collected from Kick-'em-Jenny's crater and five from a landslide deposit (Fig. 1). We infer that debris avalanche/landslide deposits represent collapsed material from one or more earlier eruptions of the respective volcanoes. We re-analysed five samples collected using grab sampling by the *H.M.S. Hecla* survey in 1972, first described in Sigurdsson and Shepherd (1974), and kindly provided by Steve Carey (University of Rhode Island). These samples were reportedly taken from various parts of the cone and crater (Sigurdsson and Shepherd, 1974). Sample collections from 1972 and 2013/14 expeditions occurred ~6 and ~12 years, respectively, after the corresponding documented eruption (Table 1). There is some duplication in names between 1972 and 2013/14 Kick-'em-Jenny samples (e.g. KEJ010, Fig. 2) used in this study. Where this occurs, the date of collection is stipulated in parentheses, e.g. KEJ010 (1972) or KEJ010 (2014).

2.2. Whole rock chemistry

Whole rock major and trace elements were analysed by X-ray fluorescence spectrometry (XRF) on twenty Kick-'em-Jenny and three Kick-'em-Jack samples using a Bruker-AXS S4 Pioneer instrument at the University of East Anglia. Samples were first crushed and powdered using a rock splitter, jaw crusher and planetary ball mill at the University of Bristol. Pressed pellets and glass beads were then prepared at the University of East Anglia for analysis. For major elements, the instrument was calibrated using the following standards: SDO-1, GSP-2, W2a, AC-E and AGV-2. For trace elements, the instrument was calibrated using the following standards: SDO-1, Mess-2, STSD-2 and W2a. Differences between measured and reference values for these standards are <0.44 wt% and <8 ppm for major and trace elements respectively.

2.3. Mineral and melt inclusion chemistry

2.3.1. Major elements

Minerals and melt inclusions (MIs) were analysed using a Cameca SX100 electron microprobe at the University of Bristol. Samples were analysed as polished, carbon-coated thin sections. Some minerals were also hand picked from coarsely crushed samples, mounted in epoxy, polished until MIs were exposed and then carbon-coated for analysis. For mineral analyses, a 20 kV accelerating voltage, 10 nA beam current and 1 μm spot were used. For MI analyses, a 20 kV accelerating voltage, 4 nA beam current and 5 μm-defocused spot were used to minimize alkali migration during analysis (Humphreys et al., 2006). Both techniques were calibrated using oxide, mineral and metal standards.

2.3.2. Trace elements and volatiles

Trace element, H_2O and CO_2 concentrations in MIs were analysed on gold-coated, polished thin sections and grain mounts by secondary ion mass spectrometry (SIMS) using the Cameca IMS4f ion-microprobe at the NERC facility, University of Edinburgh. Carbon coats were thoroughly removed prior to SIMS analysis. On any one MI, CO_2 (as $^{12}C^+$) was measured first, followed by H_2O (as $^1H^+$) and trace elements (^{7}Li, ^{11}B, ^{47}Ti, ^{88}Sr, ^{89}Y, ^{90}Zr, ^{93}Nb, ^{138}Ba, ^{140}Ce) in a separate routine. Both

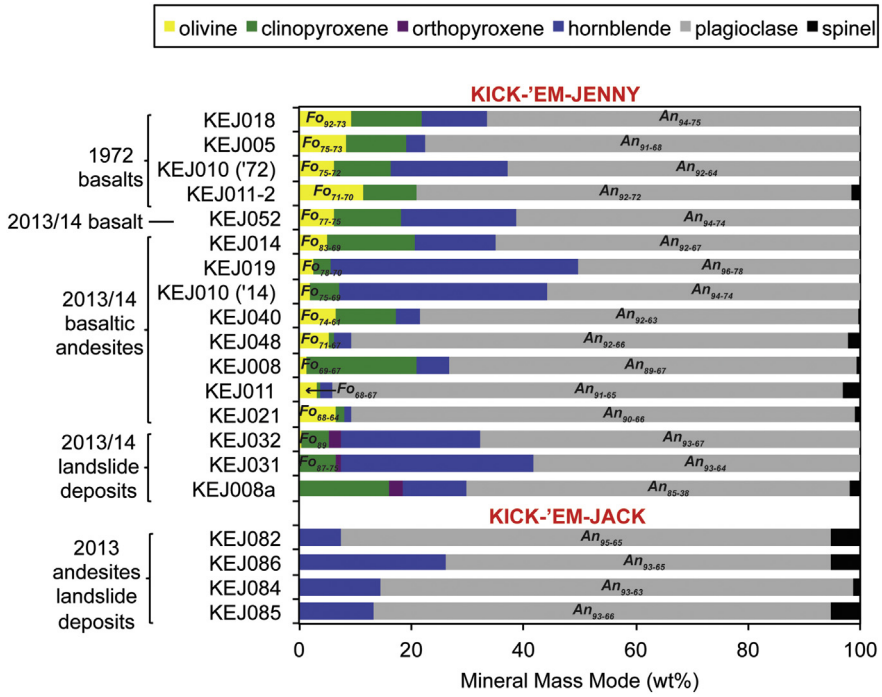

Fig. 2. Modal proportions by mass of Kick-'em-Jenny and Kick-'em-Jack phenocrysts. Samples are listed in order of decreasing Fo content of olivine followed by An content of plagioclase within a specific rock type group. 2013/14 landslide deposits consist of two basaltic andesites and one andesite (KEJ008a).

analytical routines were conducted on exactly the same area of the inclusion. Instrument conditions comprised 10 kV $^{16}O^-$ 2–5 nA primary beam focused to an ~10 μm spot on the sample surface. Positive secondary ions were extracted at 4.5 kV with an energy offset of 50 eV for CO_2 (75 eV for H_2O) and a 25 μm image field. $^{12}C^+$ data were obtained at high mass resolution to eliminate $^{24}Mg^{2+}$ interference. Volatile species were calibrated against basaltic glass standards using data analysis procedures of Blundy and Cashman (2008). Trace elements were calibrated against glass standard GSD.

3. Results

3.1. Petrography

Kick-'em-Jenny 1972 samples consist of basalts, while the 2013/14 collection consists of basalts, basaltic andesites and andesites (Fig. 2). It should be noted that non-vesicular basaltic andesites and andesites were also collected during the 1972 expedition (Devine and Sigurdsson, 1995), but were proportionally less abundant than basalts (Supplementary Fig. S1). All rock types are glomeroporphyritic and vesicular (up to 16% by volume) with phenocrysts of olivine, clinopyroxene, orthopyroxene, hornblende, plagioclase and spinel (Fig. 3a–f). Some minerals show embayed or corroded edges as well as resorption of grain interiors. Mineral textures are summarised in Table 2. Plagioclase is the most abundant phase. Hornblende and clinopyroxene are the second most abundant phases in 56% and 44% of samples respectively. Orthopyroxene is restricted to samples collected from debris avalanche deposits, while being absent from crater-derived samples. Crystal clusters, showing a variety of grain size arrangements, are ubiquitous (Fig. 3c & d). Polymineralic clusters containing two or more phases are typical, with fewer instances of monomineralic (clinopyroxene- and plagioclase-only) clots. Recrystallised interstitial glass is observed in some clusters (Fig. 3c). Some constituent minerals (e.g. hornblende) also appear to be breaking down when in contact with glass or other minerals. Kick-'em-Jenny's lavas quench upon eruption under water preventing extensive degassing and readily preserving melt inclusions in phenocryst phases.

Secondary minerals such as calcite and prehnite occupy vesicles and/or veins in some samples (Fig. 3c), suggesting that some Kick-'em-Jenny lavas were affected by low temperature burial metamorphism and seawater infiltration. The groundmass consists of microlites of spinel, olivine, plagioclase, clinopyroxene, orthopyroxene and apatite together with some glass, collectively making up some 38–70% by volume on a vesicle-free basis. The groundmass of one sample (KEJ010-2014) displays an irregular interplay of predominantly dark and light minerals suggesting compositional variability of the melt (Fig. 3f) and possibly mixing of magmas and/or entrained crystals.

Kick-'em-Jack andesites are porphyritic, consisting of mainly hornblende, plagioclase and spinel phenocrysts (Fig. 3g & h, Table 2). Olivine was observed in one sample included in a hornblende grain. Again, plagioclase is the predominant phase, followed by hornblende (Fig. 2). Glomerocrysts are less prevalent in Kick-'em-Jack lavas than in Kick-'em-Jenny lavas, but when present exhibit both poly- and monomineralic clusters (Fig. 3h). Vesicles make up ≤6% by volume. The groundmass consists of microlites of plagioclase and spinel embedded in glass making up 89–93% by volume on a vesicle-free basis.

3.2. Mineral chemistry

Full mineral composition datasets for Kick-'em-Jenny and Kick-'em-Jack lavas are presented in Supplementary Tables S1 and S2 respectively. Ferric iron contents were estimated using the stoichiometric methods of Droop (1987) for spinel, Lindsley (1983) for clinopyroxene, and Holland and Blundy (1994) for hornblende. For spinel and clinopyroxene, Mg# is expressed as 100 $Mg/(Mg + Fe^{2+})$ and for hornblende, Mg# is expressed as 100 $Mg/(Mg + Fe^{Total})$.

3.2.1. Olivine

Kick-'em-Jenny olivine phenocryst compositions range from $Fo_{92–61}$ (Fig. 2). $Fo_{<70}$ olivines are restricted to 2013/14 samples, while select 1972 (KEJ018), 2013 (KEJ014) and 2013/14 landslide deposit (KEJ031 and KEJ032) samples contain the highest Fo contents (>80) (Fig. 5). Interestingly, these samples also exhibit significant normal zoning, e.g. KEJ018 (e.g. $Fo_{92–79}$), KEJ014 (e.g. $Fo_{83–75}$) and KEJ032 (e.g. $Fo_{87–80}$)

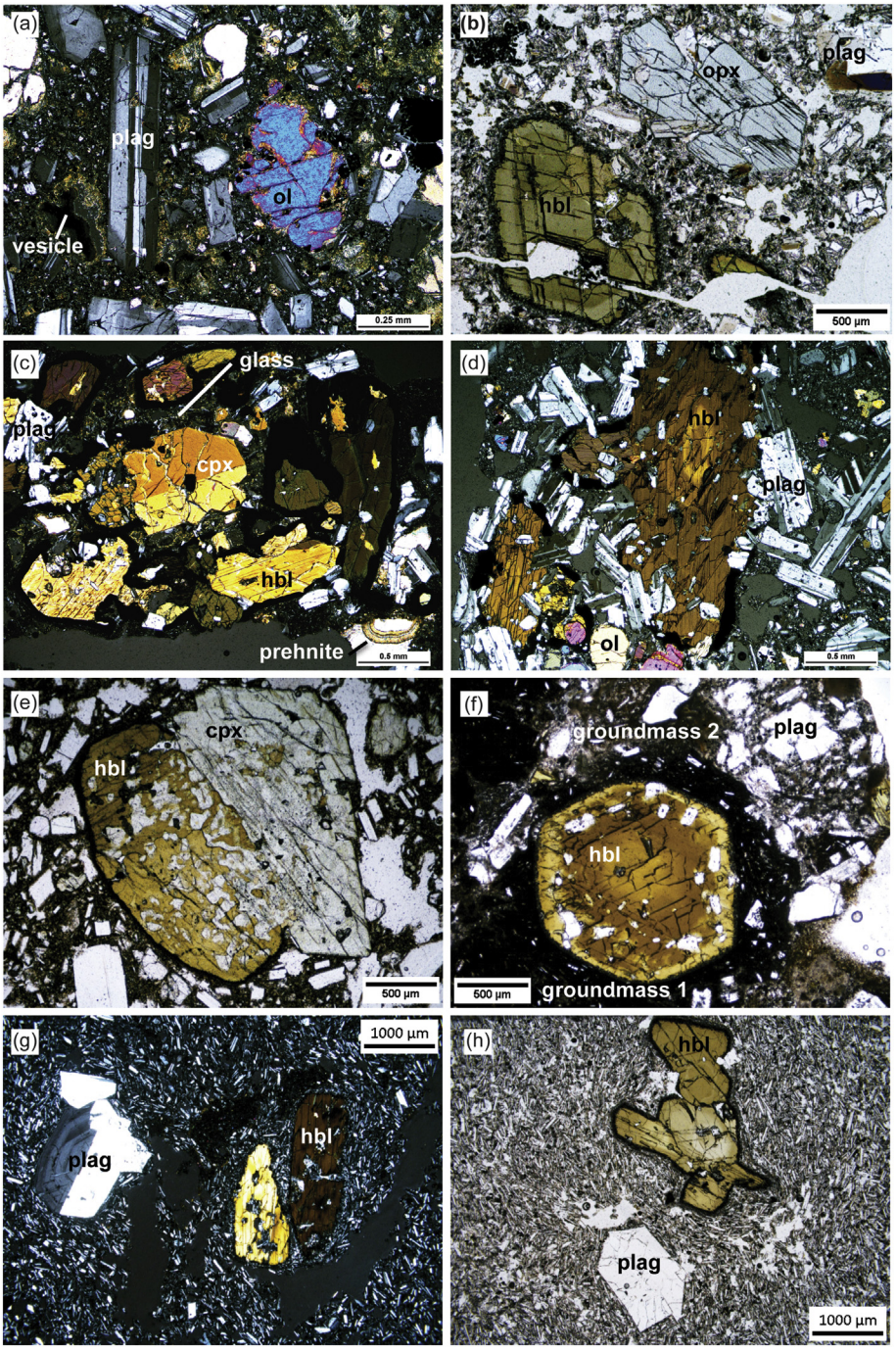

Fig. 3. Photomicrographs of representative minerals and textures in Kick-'em-Jenny (a–f) and Kick-'em-Jack lavas (g–h) (cross polarised light, xpl; plane polarised light, ppl). (a) Basaltic andesite with olivine altered along grain edges and fractures, sieve textured plagioclase and vesicles, xpl (KEJ014). (b) Basaltic andesite with orthopyroxene and zoned hornblende, xpl (KEJ031). (c) Crystal cluster with recrystallised interstitial melt, xpl (KEJ049). (d) Cluster with millimeter and micrometer sized crystals, xpl (KEJ008). (e) Crystal clot displaying varying degrees of uralitization: left crystal shows clinopyroxene mostly replaced to hornblende and right crystal showing the beginnings of clinopyroxene replacement (KEJ018), ppl. (f) Groundmass compositional variability, ppl (KEJ010, 2014). (g) Typical oscillatory-zoned plagioclase with trachytic groundmass, xpl (KEJ084). (h) Hornblende-dominated glomerocryst, ppl (KEJ086).

with the most Fo-rich compositions preserved as small, corroded grain cores with abrupt transitions to less Fo-rich rims (Fig. 4b & d). Olivine grains elsewhere (phenocrysts and glomerocrysts) are only marginally zoned (normal and reverse) showing at most a 1% Fo rimward decrease or increase (Fig. 4a). There is a steady decrease in MnO from 0.8 to 0.15 wt% with decreasing Fo (Supplementary Table S1a). NiO (0.03 to 0.50 wt%) increases with increasing Fo (Fig. 5a). Landslide deposits are distinct in their trend with higher NiO contents for a given MgO. CaO varies between 0.11 and 0.30 wt% with no discernible relationship with Fo (Fig. 5b). CaO contents are always higher in phenocryst rims compared to cores showing for the most part a rimward increase of 0.06 wt% for 1972 and 0.03 wt% for 2013/14 lavas. Phenocrysts and glomerocrysts follow a similar distribution with no significant compositional distinction. Microlite compositions range $Fo_{66–59}$, <0.02 wt% NiO and 0.34–0.41 wt% CaO (Fig. 5). Also plotted on Fig. 5b are isotherms calculated using the Ca-in-olivine thermometer of Shejwalkar and Coogan (2013) appropriate for orthopyroxene-bearing lavas KEJ031 and KEJ032.

The single olivine grain analysed from Kick-'em-Jack has Fo_{79}, CaO 0.09 wt% and NiO 0.13 wt%.

Table 2
Phenocryst petrographic descriptions for Kick-'em-Jenny and Kick-'em-Jack lavas.

Mineral phase	Volcano	Grain size & shape	Textural types	Other comments
Olivine	Kick-'em-Jenny	• <500 μm, KEJ014 < 1 mm • Subhedral & anhedral	• Isolated phenocrysts and microphenocrysts (Fig. 3a) • Clotted with spinel, clinopyroxene, orthopyroxene, hornblende and/or plagioclase (Fig. 3d)	• Zoned • Unaltered except KEJ014 (Fig. 4d) • Rare in debris avalanche deposits (<1%) forming clots with and surrounded by overgrowths of clinopyroxene, hornblende (Fig. 4c) and orthopyroxene
Clinopyroxene	Kick-'em-Jenny	• <2.5 mm • Euhedral, subhedral & anhedral	• Large isolated euhedral/subhedral grains (~2.5 mm) • Smaller isolated euhedral/subhedral grains (<2 mm) • Subhedral/anhedral grains (<2 mm) clotted with olivine, hornblende, plagioclase and/or spinel • Grains showing replacement to hornblende (Fig. 3e)	• Zoned (compositional, oscillatory and sector) • Inclusions of spinel and plagioclase
Orthopyroxene	Kick-'em-Jenny	• <2 mm • Subhedral	• Isolated grains (Fig. 3b) • Clotted with olivine, clinopyroxene and/or plagioclase	• Zoned • Present only debris avalanche deposits
Hornblende	Kick-'em-Jenny	• <5 mm • Euhedral, subhedral & anhedral	• Euhedral/subhedral isolated phenocrysts with or without inclusions of olivine, clinopyroxene, plagioclase (Fig. 3f) • Anhedral/subhedral isolated phenocrysts with fragmented/resorbed grain interiors and edges (Fig. 3b) • Clotted with plagioclase, clinopyroxene and/or orthopyroxene (Fig. 3c & d) • Grains showing uralitization of clinopyroxene to hornblende (Fig. 3e)	• Zoned phenocrysts (compositional and oscillatory), unzoned microphenocrysts • Absent from KEJ011-2 (1972) • Thick opacite reaction rims (Fig. 3b, c, d & e), few grains are completely opacitized
	Kick-'em-Jack	• <5 mm • Euhedral, subhedral & anhedral	• Large (~5 mm), isolated, euhedral/subhedral phenocrysts with/without inclusions of other phases • Smaller isolated euhedral/subhedral phenocrysts (<2 mm) with/without inclusions of other phases (Fig. 3g) • Anhedral/subhedral phenocrysts clotted with other hornblende grains and/or other phases (Fig. 3h)	• Zoned phenocrysts, unzoned microphenocrysts • Opacite rims (Fig. 3h)
Plagioclase	Kick-'em-Jenny	• <2.5 mm • Subhedral	• Large isolated phenocrysts (~2–2.5 mm) with thinly zoned rims • Isolated phenocrysts & microphenocrysts (<2 mm) (Fig. 3a) • Clotted with other minerals (Fig. 3c & d)	• Zoned (oscillatory only in isolated phenocrysts) • Sieve textured cores (except some microphenocrysts) • Minor spinel, olivine and hornblende inclusions
	Kick-'em-Jack	• <2 mm • Subhedral	• Isolated phenocrysts/microphenocrysts • Clotted with other plagioclase grains, hornblende and/or spinel	• Zoned (oscillatory) (Fig. 3g) • Sieve textured cores
Spinel (magnetite-rich)	Kick-'em-Jenny & Kick-'em-Jack	• <200 μm • Subhedral & anhedral	• Isolated • Clotted with other phases	• Included in all phases

3.2.2. Pyroxene

All textural types of phenocryst clinopyroxene (Table 2) in Kick-'em-Jenny lavas have diopside and high-Ca augite compositions with $Mg\#_{93–71}$ (Supplementary Table S1c). Zoning is ubiquitous with analyses from both time periods displaying normal (maximum 15 mol% rimward decrease, e.g. KEJ018 $Mg\#_{88–73}$) and reverse (maximum 6 mol% rimward increase, e.g. KEJ005, $Mg\#_{79–85}$) zoning. Ca content in clinopyroxene increases (0.73–0.93 p.f.u.) with decreasing Mg#, but there is no clear chemical distinction between phenocrysts and glomerocrysts for either 1972 or 2013/14 deposits. Al^{IV} contents vary between 0.04 and 0.24 p.f.u. and TiO_2 varies between 0.2 and 1.1 wt%. There is no clear correlation between Mg# and Al^{IV} or TiO_2. Microlite compositions are also diopside and high-Ca augite, mirroring trends of phenocryst Ca (0.60–0.85 p.f.u.), Al^{IV} (0.01–0.19 p.f.u.) and TiO_2 (0.2–1.5 wt%) with Mg# ($Mg\#_{100–63}$).

Phenocryst and microlite orthopyroxene for Kick-'em-Jenny lavas are enstatite in composition ($Mg\#_{78–67}$ and $Mg\#_{75–68}$ respectively) (Supplementary Table S1d). Normally zoned phenocrysts display up to a 5 mol% rimward decrease in Mg# (e.g. $Mg\#_{77–72}$, KEJ031). Phenocryst Al^{IV} compositions (0.01–0.11) increase with increasing Mg#, while Ca (p.f.u.) and Ti (p.f.u.) compositions show no discernible pattern with Mg#, with contents of <0.10 and <0.16 respectively. Microlite Al^{IV} compositions (<0.03) also increase with increasing Mg#, while Ca (<0.06 p.f.u.) and TiO_2 (<0.3 wt%) compositions show no discernible pattern with Mg#.

3.2.3. Hornblende

Phenocryst hornblendes in Kick-'em-Jenny and Kick-'em-Jack lavas are pargasite according to Leake et al. (2003) with Mg# ranges of 80–62 and 79–63 respectively (Supplementary Tables S1e and S2c). For Kick-'em-Jenny, normally zoned phenocrysts show up to a 9% Mg# rimward decrease, e.g. $Mg\#_{89–80}$, KEJ008 (up to 4% for Kick-'em-Jack glomerocrysts, e.g. $Mg\#_{89–85}$, KEJ085), while reversely zoned grains show up to a 11% Mg# rimward increase, e.g. $Mg\#_{83–94}$, KEJ032 (up to 9% for Kick-'em-Jack glomerocrysts, e.g. $Mg\#_{84–93}$). A striking feature of Kick-'em-Jenny and Kick-'em-Jack hornblendes are their high Al_2O_3 contents (10.7–15.6 wt%). Samples from both volcanoes show a decrease in K and Al^{IV} with decreasing Mg# (Fig. 6a & c). Most samples display a fairly constant Ti concentration with changing Mg#, while a subset of 1972 and 2013/14 edifice deposits display a contrasting trend of decreasing Ti content with increasing Mg# (Fig. 6b). 1972 and 2013/14 edifice deposit hornblendes have distinct compositions in terms of K, Ti and Al^{IV}, from 2013/14 landslide deposit and Kick-'em-Jack hornblendes (Fig. 6a, b & c). These components are consistently lower in concentration in Kick-'em-Jack and 2013/14 landslide deposits compared to the rest of Kick-'em-Jenny samples.

3.2.4. Plagioclase

Phenocryst plagioclase in both Kick-'em-Jenny and Kick-'em-Jack volcanoes is predominantly anorthitic ($An_{96–64}$), with only 2013/14 landslide deposits exhibiting An contents <64 (Fig. 7). Microlite compositions range $An_{79–46}$. Iron concentrations increase with An content until about An_{65}, after which Fe contents decrease with increasing An content. This behaviour mimics the onset of magnetite saturation observed in whole rocks (see below). Potassium concentrations decrease with increasing An content. As with other phases, there is no discernible chemical distinction between phenocrysts and glomerocrysts. The large isolated plagioclase phenocrysts have a propensity for An contents ≥90.

There is a significant difference in the extent of normal zoning between 1972 and 2013/14 phenocrysts: 1972 plagioclase display cores ranging from $An_{94–84}$ while plagioclase cores from 2013/14 range

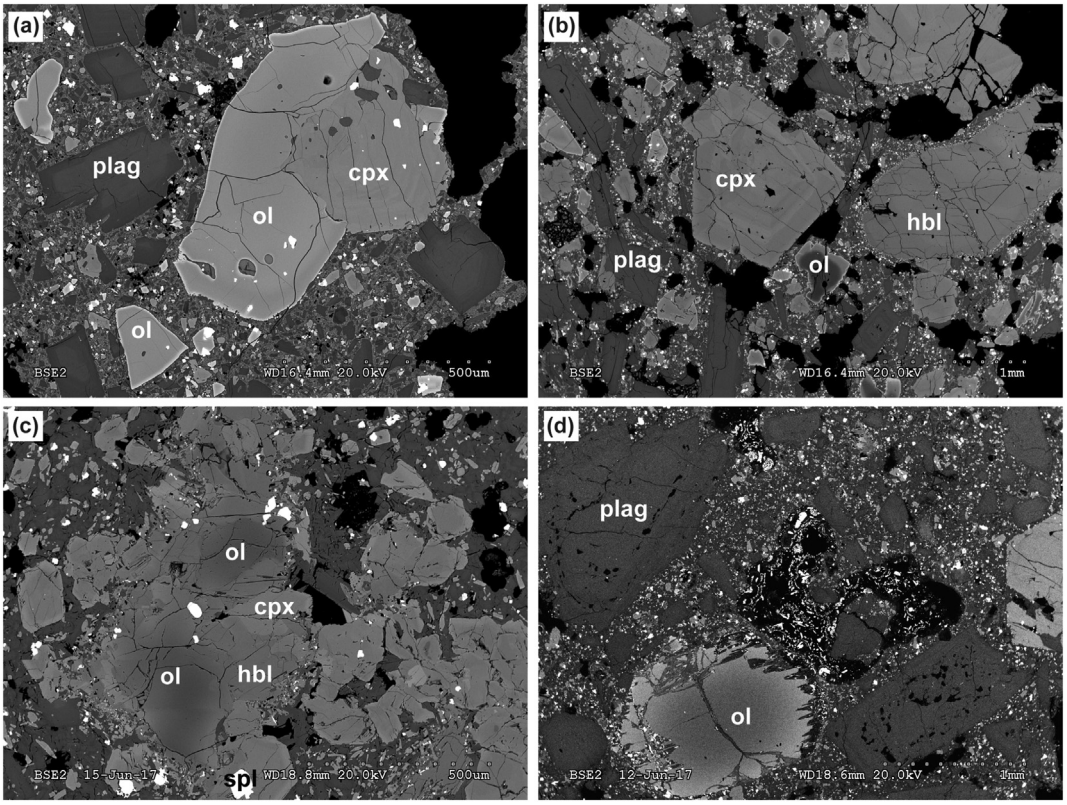

Fig. 4. Backscattered electron images highlighting olivine textures and zoning in Kick-'em-Jenny lavas. (a) Isolated and clotted olivine with thinly zoned rims (KEJ010, 1972). (b) Isolated phenocrysts of zoned olivine, clinopyroxene, hornblende and plagioclase (KEJ018). (c) Zoned olivine clotted with overgrowth minerals of hornblende and clinopyroxene (KEJ032). (d) Zoned olivine (altered rim) and plagioclase (sieve textured) (KEJ014).

from $An_{96-69,}$ with rim variations of An_{87-68} and An_{91-63} respectively. Plagioclase phenocrysts from 2013/14 landslide deposits exhibit even wider variations in An content: cores An_{93-49}, rims An_{85-38}. There is much more compositional variability in 2013/14 edifice samples compared to 1972. Normally zoned Kick-'em-Jack plagioclases have cores An_{94-75} and rims An_{88-65} that are similar in terms of compositional variation to Kick-'em-Jenny 1972 samples. Reverse zoning was not observed in Kick-'em-Jenny 1972 or 2013/14 landslide deposits. However, in 2013/14 edifice deposits, rimward increases of up to a 9% An are observed.

3.2.5. Spinel

Spinel compositions are predominantly titaniferous magnetite (Supplementary Fig. S2). 2013/14 landslide deposit and Kick-'em-Jack spinels are distinct from 1972 and 2013/14 edifice deposit spinels in terms of Ti content. Chrome-rich spinels are observed in a few 2013/14 landslide deposits (Cr# >60) as inclusions in hornblende, clinopyroxene and olivine (Fo_{82}), in glomerocrysts or as isolated grains (Supplementary Fig. S2).

3.3. Whole-rock chemistry

Selected major and trace element variations in Kick-'em-Jenny and Kick-'em-Jack lavas are shown on MgO plots in Figs. 8 and 9. Full datasets for Kick-'em-Jenny and Kick-'em-Jack lavas are presented in Supplementary Table S3. Whole-rock data for 1972 lavas shown on Figs. 8 and 9 are taken from Sigurdsson and Shepherd (1974) and Devine and Sigurdsson (1995).

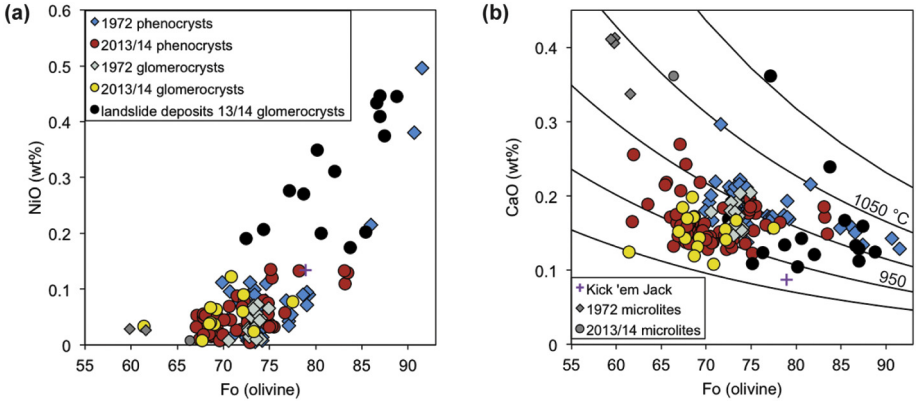

Fig. 5. Composition of Kick-'em-Jenny and Kick-'em-Jack olivine phenocrysts and glomerocrysts. (a) Forsterite content decreases steadily with NiO. The highest NiO contents are recorded in 1972 and 2013/14 landslide deposits. (b) Variation in CaO with Fo. Isolines calculated using the Ca-in-olivine thermometer of Shejwalkar and Coogan (2013) for orthopyroxene bearing lavas (KEJ031 and KEJ032).

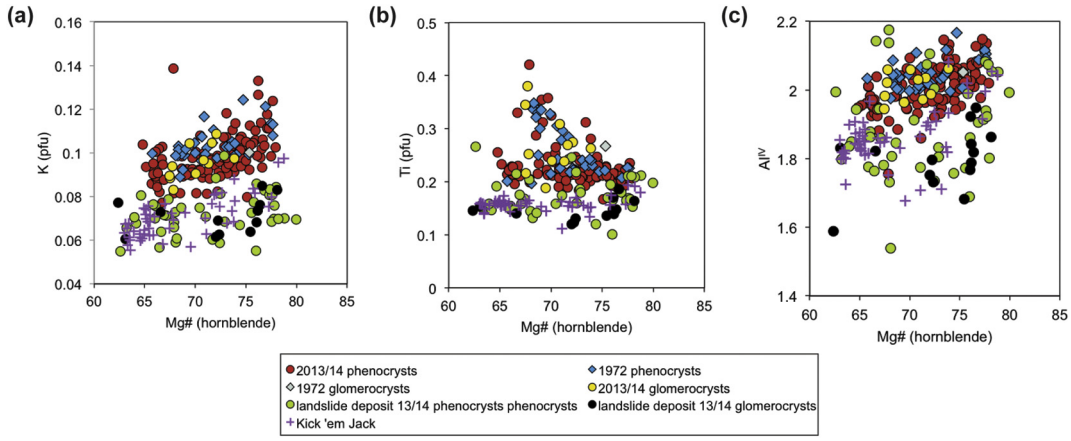

Fig. 6. Variation in hornblende composition for Kick-'em-Jenny and Kick-'em-Jack lavas. 2013/14 landslide deposit and Kick-'em-Jack samples are broadly distinct from 1972 and 2013/14 edifice deposits.

Kick-'em-Jenny lavas range from medium-K basalts to andesites (46.5–61.5 wt% SiO_2) with MgO contents of 2.5 to 12.7 wt%. In general, lavas define a plausible liquid line of descent with increasing SiO_2, alkalis and FeO_{Total} with decreasing MgO and inflections in Al_2O_3 and CaO at around 4.5 wt% MgO, consistent with the appearance of plagioclase on the liquidus (Fig. 8). However, there are distinct differences between the three datasets presented (1972, 2013/2014 and 2013/2014 landslide deposits). Lavas collected from 1972 cover a wider range of compositions from high-MgO (12.7 wt%) basalts to basaltic andesites whereas post-1972 deposits are predominantly basaltic andesite, with minor basalts. 2013/2014 lavas extend to higher Al_2O_3 at a given MgO (Fig. 8c), than the other two types of deposits. CaO, and to a lesser extent Al_2O_3, show two prominent kinks at around 8 and 10 wt% MgO (Fig. 8b). Samples from 2013/14 landslide deposits produce distinct trends for SiO_2, CaO, Al_2O_3 and FeO_{Total}. They show higher SiO_2 and lower CaO and Al_2O_3 at given MgO compared to crater deposits from 1972 and 2013/14. The FeO_{Total} is considerably lower in samples from 2013/14 landslide deposits along a trend parallel to lavas.

Lava trace elements also display fractionation trends with MgO wt%. Rb, Zr, Ba, Sr concentrations decrease with increasing MgO (Fig. 9), with 1972 and 2013/14 samples having the lowest and highest concentrations of these elements respectively. The Ba signature displays two parallel trends for 1972 and 2013/2014 crater deposits, while landslide deposits bridge these two parallel trends. Nickel and Cr (Fig. 9d and Cr in Supplementary Table S3b) concentrations decrease with decreasing MgO, with Ni reaching 232 ppm in most primitive samples. Cr contents were not measured in 1972 samples by Devine and Sigurdsson (1995). Yttrium shows an apparent maximum at around 8 wt% MgO. At lower MgO contents, Y decreases slightly, indicative of mildly compatible behaviour during differentiation. Although samples are phenocryst-rich, mass modes of the majority of phenocryst phases do not show any obvious correlation with whole rock incompatible trace element (Zr, Rb, Ba) compositions (Supplementary Fig. S3).

3.4. Glass chemistry

Melt inclusion (MI) hosts include olivine, clinopyroxene and hornblende. Inclusions range in size from <10 to 50 μm. Only glassy, transparent MIs without daughter minerals were selected for analysis. MIs have pale brown colour in transmitted light and vary in shape from rounded to oval. While vapour bubbles are common, some MIs are bubble-free. Bubbles may contain substantial concentrations of CO_2, which may lead to underestimates of the original concentration of dissolved CO_2 if analysing only the glass (Moore et al., 2015). MI major element compositions are reported in Table 3 and trace element chemistry in Supplementary Table S4. Post entrapment crystallisation (PEC) for MIs was up to 22% with approximately 75% of analyses having PEC corrections <10%. These corrections were based on comparisons of measured Kd_{Fe-Mg} values to equilibrium Kd_{Fe-Mg} values of 0.28 for clinopyroxene and 0.31 for hornblende hosts (from Run 3-1, Melekhova et al., 2017), with FeO = FeO_{Total}. For olivine hosts, we used an equilibrium value of 0.22, which represents the average $Kd_{FeTotal-Mg}$ calculated for Kick-'em-Jenny lavas of Sigurdsson and Shepherd (1974) for which Fe_2O_3 and FeO were analysed separately. However, since PEC is generally small, we have only incorporated PEC corrections for olivine hosted MIs to the dataset (Table 3). We did not find any well preserved MIs from Kick-'em-Jack or Kick-'em-Jenny landslide deposits samples.

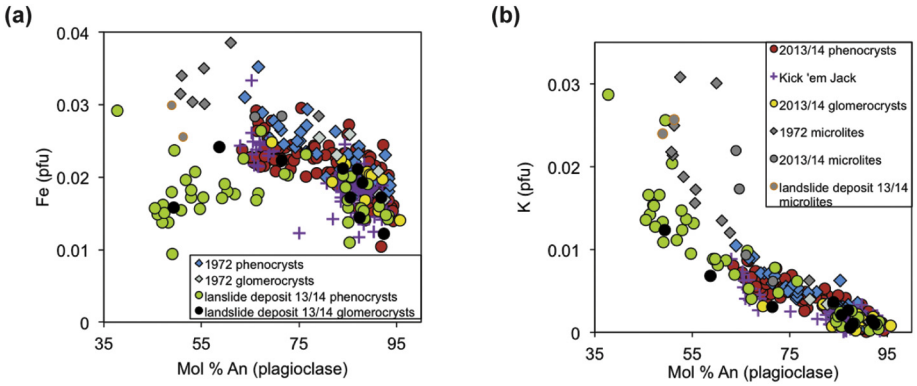

Fig. 7. Variation in plagioclase composition for Kick-'em-Jenny and Kick-'em-Jack lavas.

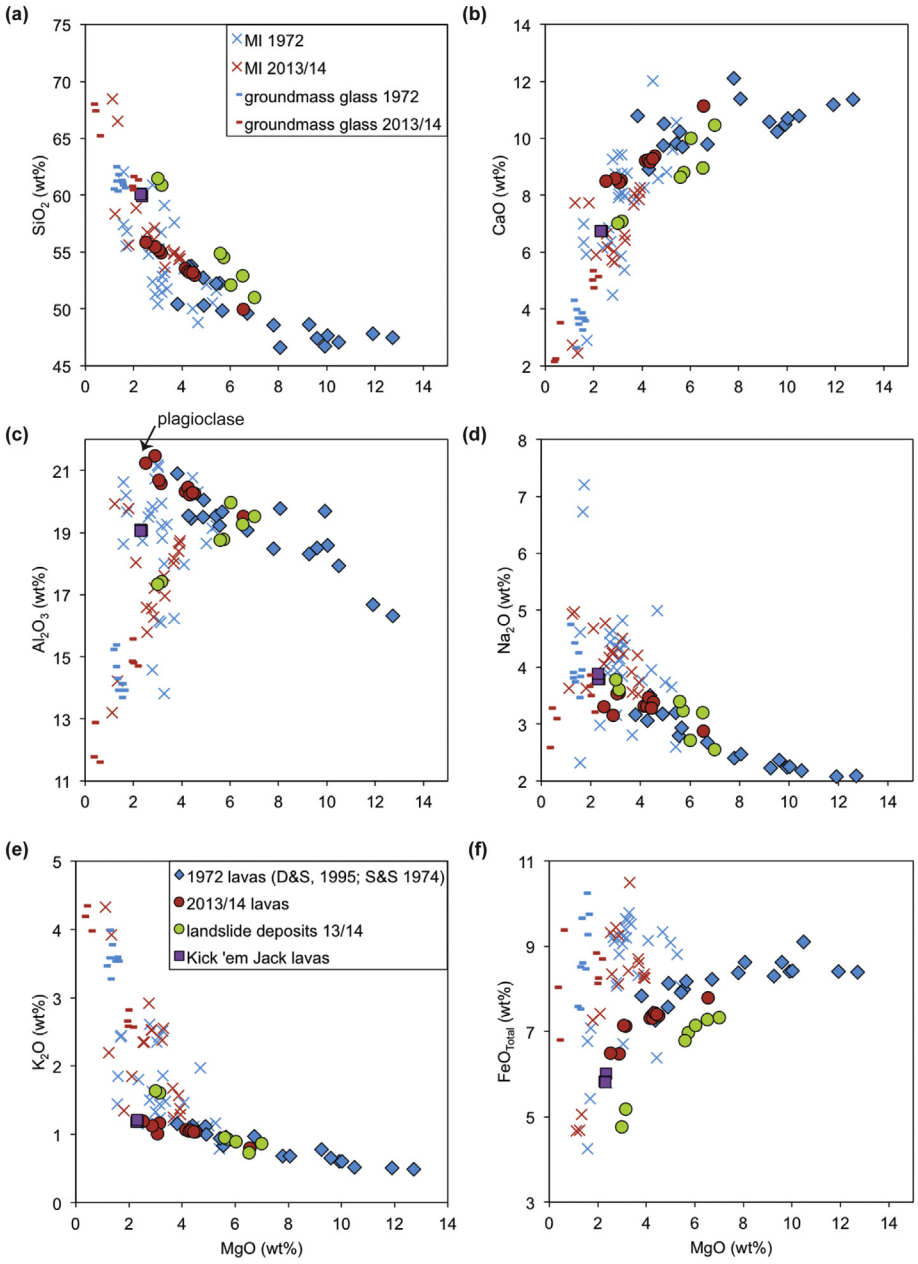

Fig. 8. Bulk-rock major element chemistry of Kick-'em-Jenny and Kick-'em-Jack lavas, melt inclusions and groundmass from this study, Sigurdsson and Shepherd (1974) (S&S, 1974) and Devine and Sigurdsson (1995) (D&S, 1995). Olivine-hosted melt inclusions are corrected for post-entrapment crystallisation. Vector added showing onset of plagioclase crystallisation.

We selected twenty-seven glassy MIs (≥30 μm in diameter) from Kick-'em-Jenny 1972 lavas and seventeen from 2013/14 lavas for analysis (Table 3). MI compositions (normalized to 100% volatile-free) vary from basalt to dacite with 1.6 to 5.4 wt% MgO for 1972 and 0.5 to 3.9 wt% MgO for 2013/14 (Fig. 8). PEC-corrected MgO contents range 2.1 to 5.5 wt% for 1972 and 1.1 to 4.8 wt% for 2013/14. Chlorine contents range from 2200 to 8800 ppm; sulphur contents up to 2100 ppm. There is no compositional difference between MIs trapped in any host phase. The most evolved MIs for 1972 and 2013/14 are found in clinopyroxene and olivine hosts respectively, with those from 2013/14 having the most evolved MIs for the entire series. Some samples contain MIs with varied melt compositions, for example, basalt, basaltic andesite and andesite melts were analysed in sample KEJ010-1972 (Table 3).

Groundmass glasses (normalized to anhydrous) range from 60 to 68 wt% SiO_2 with <2.1 wt% MgO (Fig. 8, Supplementary Table S5). As for MIs, 2013/14 groundmass glasses are more evolved than 1972. For the most part, groundmass glasses and MIs follow a linear trend towards bulk rock compositions.

Volatile concentrations (measured by SIMS) range from 0.2 to 5.0 wt % H_2O and ≤3157 ppm CO_2. Volatile contents are only minimally affected by PEC corrections. The highest CO_2 contents are found in hornblende and olivine hosts (Fig. 12). MIs contained in clinopyroxene and hornblende tend to have higher H_2O concentrations (>4 wt%) than those in olivine. Olivine hosts contain $Fo_{87–65}$. H_2O correlates fairly well with some major elements: FeO, K_2O, Na_2O and TiO_2 generally decrease with increasing H_2O, while CaO and Al_2O_3 increase. The variation in H_2O with SiO_2 shows trends consistent with decompression crystallisation and syn-eruptive degassing as described by Blundy and Cashman (2005) (Fig. 10c).

Most trace elements (B, Ti, Y, Zr, Nb, Ba, Ce) show steady low concentrations at high H_2O contents (Supplementary Table S4 and Fig. 10a) with sudden inflections below ~5 wt% MgO (Fig. 9a, b, c & f), similar to the behaviour of K_2O (Fig. 8e). Strontium shows the opposite behaviour

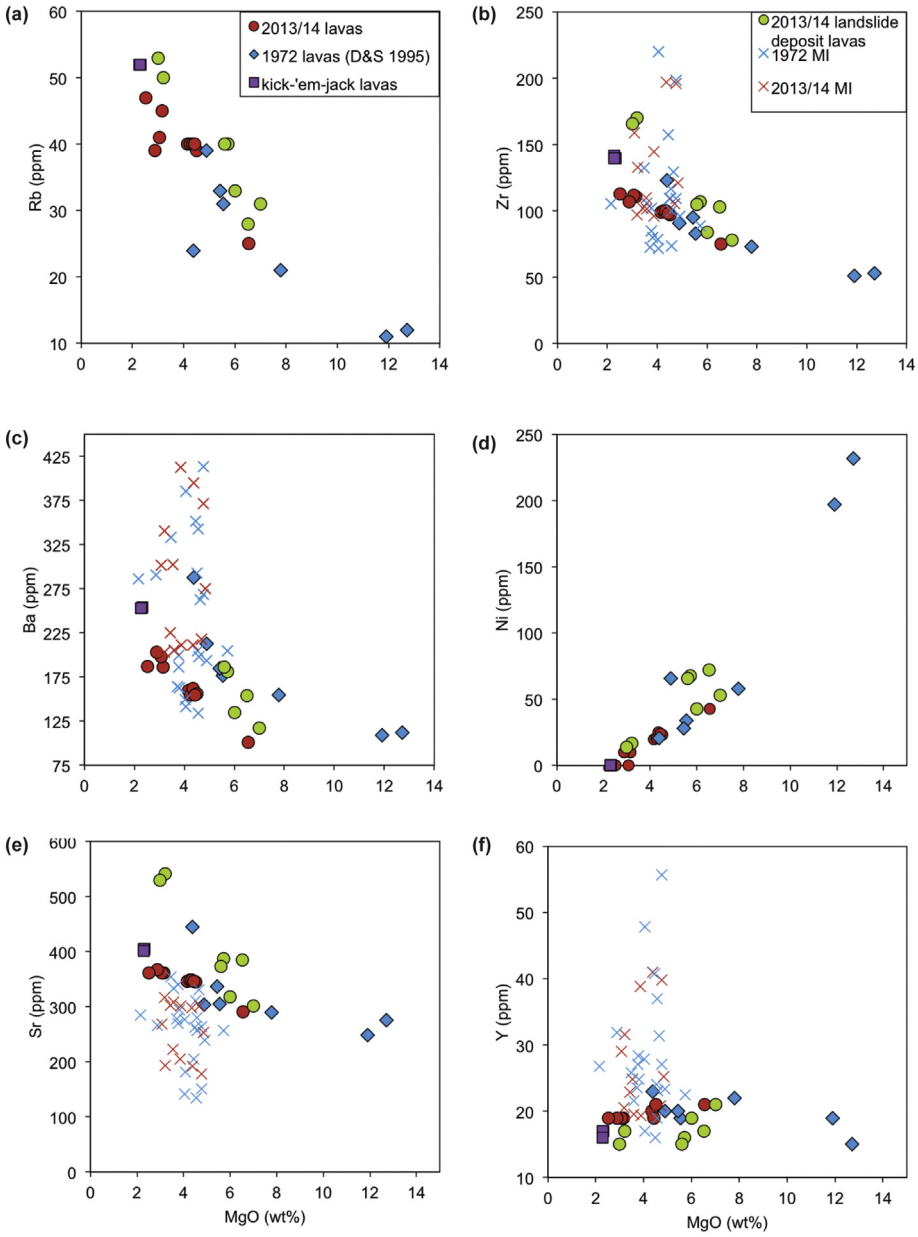

Fig. 9. Bulk-rock trace element chemistry of Kick-'em-Jenny and Kick-'em-Jack lavas and melt inclusions from this study and Devine and Sigurdsson (1995) (D&S, 1995).

(Fig. 10b), with a marked drop in concentration below 5 wt% MgO (Fig. 9e), similar to Al_2O_3 (Fig. 8a), and consistent with the onset of plagioclase crystallisation.

3.5. Intensive parameters

3.5.1. Thermometry of lavas

Mineral, MI and groundmass glass compositions were used to determine pre-eruptive magma storage conditions (P-T-H_2O-$fO2$) for Kick-'em-Jenny and Kick-'em-Jack. A combination of geothermometers was used to estimate equilibrium temperatures of phenocryst assemblages: hornblende-plagioclase (Holland and Blundy, 1994), clinopyroxene-orthopyroxene (Brey and Kohler, 1990; Putirka, 2008) and clinopyroxene-liquid (Putirka, 2008). We chose three MIs with *Kd* values indicating that PEC effects were minimal for the clinopyroxene-liquid calculations. Major element data for touching rims and/or included phases were used in hornblende-plagioclase calculations to ensure a close approach to textural equilibrium in zoned phases. Because pressure has been shown to have a modest dependence on thermometry (±72 °C/ GPa) at sub-volcanic pressures (Blundy and Cashman, 2008), a nominal value of 500 MPa was applied. The hornblende-plagioclase thermometer requires plagioclase to be less calcic than An_{90} (Holland and Blundy, 1994). Both Kick-'em-Jenny and Kick-'em-Jack contained plagioclase with higher anorthite contents, however only temperatures calculated for An <90% are included in Table 4. Clinopyroxene and orthopyroxene grains were never adjacent, therefore all combinations of individual clinopyroxene and orthopyroxene rims were used for calculations and the resulting temperatures averaged. Standard deviations for these calculations were <13 °C for KEJ031, <17 °C for KEJ032 and <59 °C for KEJ008a. Estimates of magmatic temperatures at lower pressures (i.e. eruption temperatures) were obtained using groundmass olivine-liquid assemblages (Putirka, 2008). Again, temperatures were averaged from all combinations of olivine and glass in each sample (standard deviations: 10 °C for KEJ018, 22 °C for KEJ005, 17 °C for KEJ010 (1972) and 7 °C for KEJ019).

For Kick-'em-Jenny, the temperature range obtained using the hornblende-plagioclase thermometer is lower for 1972 crater lavas

Table 3
Kick-'em-Jenny phenocryst-hosted melt inclusion compositions.

Sample	KEJ010	KEJ010	KEJ010	KEJ010	KEJ010	KEJ010	KEJ005	KEJ005	KEJ005	KEJ005	KEJ018
Name	kej010mi2ats	kej010mi10ats	kej010mi10bts	kej010mi10cts	kej010mi16ts	kej010mi22ts	kej005mi5	kej005mi20	kej005mi21b	kej005mi9	kej018mi1b
Host	ol	ol	ol	ol	ol	ol	ol	ol	ol	ol	ol
Period	1972	1972	1972	1972	1972	1972	1972	1972	1972	1972	1972
SiO_2	60.46	50.86	56.71	55.44	59.99	52.19	51.85	52.11	51.40	50.62	49.30
TiO_2	1.87	1.21	1.74	1.84	2.18	1.24	1.41	1.13	1.36	1.40	1.20
Al_2O_3	14.73	19.19	16.54	16.64	14.42	19.19	19.97	17.88	19.44	19.99	21.11
FeO	7.50	9.05	8.89	8.53	9.10	8.70	7.63	9.05	8.60	8.63	5.95
MnO	0.14	0.23	0.27	0.21	0.23	0.20	0.19	0.19	0.15	0.11	0.16
MgO	1.80	2.67	1.74	1.68	1.73	1.58	1.91	2.55	1.79	2.23	2.80
CaO	4.53	8.75	6.02	8.28	5.59	8.23	9.32	7.91	8.85	9.44	12.20
Na_2O	4.64	4.38	4.23	4.06	4.01	4.52	4.46	4.78	4.39	4.17	4.01
K_2O	2.64	1.47	2.49	2.42	2.62	1.59	1.51	1.85	1.46	1.24	1.13
P_2O_5	0.41	0.18	0.18	0.21	0.34	0.11	0.16	0.14	0.15	0.08	0.18
SO_2	bdl	0.07	bdl	0.07	0.05	0.07	0.07	0.04	0.11	0.04	0.08
Cl	0.60	0.40	0.66	0.33	0.68	0.40	0.46	0.45	0.41	0.38	0.39
Cr_2O_3	bdl	bdl	bdl	bdl	bdl	bdl	bdl	bdl	bdl	bdl	bdl
H_2O	0.53	0.85	0.45	0.65	0.50	1.68	0.38	1.04	1.31	1.36	0.72
sd	0.01	0.02	0.01	0.01	0.01	0.05	0.01	0.02	0.04	0.03	0.02
CO_2	93	bdl	bdl	43	bdl	221	67	204	137	834	459
sd	9	–	–	10	–	16	17	50	24	120	63
P_{sat}	19	10	3	13	4	72	16	49	47	205	125
Total	99.85	99.31	99.92	100.36	101.44	99.70	99.35	99.12	99.43	99.69	99.23
Restored compositions											
SiO_2	59.87	50.63	55.97	54.77	59.03	51.57	51.52	51.84	50.91	50.29	48.94
TiO_2	1.82	1.19	1.68	1.77	2.08	1.18	1.38	1.11	1.31	1.37	1.16
Al_2O_3	14.34	18.85	15.89	16.00	13.79	18.36	19.50	17.55	18.73	19.50	20.33
FeO	7.93	9.31	9.51	9.14	9.77	9.38	8.01	9.33	9.17	9.00	6.25
MnO	0.15	0.24	0.28	0.22	0.24	0.21	0.20	0.19	0.16	0.11	0.16
MgO	2.73	3.31	3.09	3.03	3.28	3.12	2.73	3.20	3.08	3.10	4.34
CaO	4.42	8.60	5.79	7.97	5.36	7.88	9.11	7.76	8.53	9.21	11.75
Na_2O	4.52	4.30	4.06	3.91	3.84	4.33	4.36	4.69	4.23	4.06	3.86
K_2O	2.57	1.45	2.39	2.33	2.51	1.52	1.48	1.81	1.41	1.21	1.09
Cr_2O_3	0.00	0.00	0.00	0.00	0.00	0.00	0.02	0.00	0.01	0.00	0.00

Sample	KEJ005	KEJ010	KEJ010	KEJ010	KEJ010	KEJ010	KEJ018	KEJ009	KEJ009	KEJ010	KEJ009
Name	kej005mi21a	kej010mi6ts	kej010mi12ts	kej010mi7	kej010mi9	kej010mi8	kej018mi3	kej009mi3a	kej009mi3b	kej010mi6a	kej009mi6
Host	ol	ol	cpx	cpx	cpx	cpx	cpx	cpx	cpx	cpx	hbl
Period	1972	1972	1972	1972	1972	1972	1972	1972	1972	1972	1972
SiO_2	50.63	49.61	56.53	58.07	48.08	56.05	53.02	54.20	54.06	53.96	49.80
TiO_2	1.13	1.10	1.21	0.51	0.96	1.02	1.01	0.80	0.89	1.18	1.02
Al_2O_3	20.94	21.23	19.57	19.30	17.92	17.44	17.19	19.26	19.13	15.22	18.86
FeO	8.12	8.47	7.04	3.98	7.52	5.39	6.26	9.11	8.89	7.78	8.68
MnO	0.11	0.14	0.16	0.15	0.19	0.12	0.19	0.18	0.20	0.28	0.25
MgO	1.76	2.09	1.71	1.47	5.05	2.20	1.46	2.59	2.63	3.45	5.18
CaO	8.84	9.44	2.89	5.94	9.82	5.71	6.46	6.77	6.20	7.36	9.47
Na_2O	4.69	4.38	7.16	2.17	2.43	2.78	4.25	3.97	3.79	2.63	3.60
K_2O	1.64	1.33	2.43	1.35	0.73	1.67	1.71	1.16	1.12	1.12	1.15
P_2O_5	0.20	0.14	0.20	0.09	0.14	0.28	0.22	0.22	0.20	0.20	0.14
SO_2	0.12	0.11	0.06	0.19	0.13	0.05	0.05	0.08	0.07	0.14	0.05
Cl	0.37	0.37	0.48	0.34	0.22	0.42	0.44	0.43	0.35	0.33	0.32
Cr_2O_3	bdl	bdl	bdl	bdl	bdl	bdl	bdl	bdl	bdl	bdl	bdl

(continued on next page)

Table 3 (*continued*)

Sample	KEJ005	KEJ010	KEJ010	KEJ010	KEJ010	KEJ010	KEJ018	KEJ009	KEJ009	KEJ010	KEJ009
Name	kej005mi21a	kej010mi6ts	kej010mi12ts	kej010mi7	kej010mi9	kej010mi8	kej018mi3	kej009mi3a	kej009mi3b	kej010mi6a	kej009mi6
Host	ol	ol	cpx	cpx	cpx	cpx	cpx	cpx	cpx	cpx	hbl
Period	1972	1972	1972	1972	1972	1972	1972	1972	1972	1972	1972
H_2O	0.83	0.20	1.67	3.54	5.02	4.34	3.44	1.35	3.07	4.53	1.65
sd	0.02	0.02	0.04	0.20	0.11	0.12	0.09	0.03	0.12	0.10	0.03
CO_2	666	56	bdl	439	784	694	75	bdl	bdl	767	bdl
sd	33	21	–	43	29	57	40	–	–	38	–
P_{sat}	164	15	31	185	325	258	105	21	87	273	35
Total	99.38	98.61	101.11	97.10	98.21	97.47	95.74	100.17	100.40	98.21	100.19
Restored compositions											
SiO_2	50.23	49.34	–	–	–	–	–	–	–	–	–
TiO_2	1.09	1.07	–	–	–	–	–	–	–	–	–
Al_2O_3	20.30	20.71	–	–	–	–	–	–	–	–	–
FeO	8.63	8.86	–	–	–	–	–	–	–	–	–
MnO	0.12	0.15	–	–	–	–	–	–	–	–	–
MgO	2.82	2.95	–	–	–	–	–	–	–	–	–
CaO	8.58	9.21	–	–	–	–	–	–	–	–	–
Na_2O	4.55	4.27	–	–	–	–	–	–	–	–	–
K_2O	1.59	1.30	–	–	–	–	–	–	–	–	–
Cr_2O_3	0.00	0.00	–	–	–	–	–	–	–	–	–

Sample	KEJ009	KEJ011	KEJ011	KEJ005	KEJ009	KEJ050	KEJ042	KEJ042	KEJ019	KEJ019	KEJ019
Name	kej009mi4	kej011mi3a	kej011mi3b	kej005mi22b	kej009mi5	kej050mi16	kej042mi13	kej042mi9	kej019mi20	kej019mi22a	kej019mi21b
Host	hbl	hbl	hbl	hbl	hbl	ol	ol	ol	ol	hbl	hbl
Period	1972	1972	1972	1972	1972	2013	2013	2013	2014	2014	2014
SiO_2	48.05	51.62	51.52	54.30	52.15	65.84	67.11	57.89	57.21	54.39	55.49
TiO_2	0.82	0.98	0.93	0.98	0.94	1.47	1.73	0.84	0.89	0.62	2.19
Al_2O_3	20.00	17.32	19.67	19.76	18.64	14.14	13.07	20.03	17.55	19.34	15.44
FeO	9.19	8.80	6.26	5.31	9.09	4.75	4.09	4.16	7.19	7.11	8.17
MnO	0.12	0.26	0.12	0.18	0.21	0.09	0.09	0.08	0.19	0.13	0.21
MgO	4.61	3.93	2.82	1.64	5.00	0.10	0.53	0.58	1.99	1.76	2.52
CaO	8.45	7.98	7.39	5.79	8.82	2.44	2.70	7.78	5.75	7.57	6.05
Na_2O	4.91	3.63	2.93	6.58	3.74	4.95	3.59	4.97	4.55	3.55	4.67
K_2O	1.94	1.41	0.99	2.38	1.12	3.91	4.28	2.20	1.80	1.32	2.30
P_2O_5	0.10	0.14	0.10	0.23	0.11	0.51	0.53	0.28	0.13	0.21	0.23
SO_2	bdl	0.05	0.19	0.06	bdl	bdl	0.04	0.06	0.04	0.03	0.03
Cl	0.24	0.32	0.24	0.59	0.22	0.76	0.87	0.57	0.51	0.32	0.57
Cr_2O_3	bdl	bdl	bdl	bdl	bdl	bdl	bdl	bdl	bdl	bdl	bdl
H_2O	1.06	3.29	4.01	2.11	1.30	0.56	1.05	0.44	3.19	3.39	1.41
sd	0.02	0.10	0.25	0.05	0.04	0.02	0.03	0.01	0.07	0.09	0.03
CO_2	bdl	246	663	145	bdl	2513	854	311	165	102	3157
sd	–	20	76	7	–	250	154	81	52	71	847
P_{sat}	15	133	253	66	20	552	164	91	114	116	513
Total	99.54	99.73	97.18	99.91	101.35	99.52	99.68	99.88	101.01	99.74	99.28
Restored compositions											
SiO_2	–	–	–	–	–	65.56	66.57	57.50	57.19	–	–
TiO_2	–	–	–	–	–	1.45	1.70	0.83	0.89	–	–
Al_2O_3	–	–	–	–	–	14.00	12.83	19.64	17.53	–	–
FeO	–	–	–	–	–	4.98	4.54	4.63	7.21	–	–
MnO	–	–	–	–	–	0.10	0.10	0.09	0.19	–	–
MgO	–	–	–	–	–	1.32	1.09	1.23	2.04	–	–
CaO	–	–	–	–	–	2.42	2.66	7.63	5.74	–	–
Na_2O	–	–	–	–	–	4.90	3.53	4.87	4.54	–	–

K_2O	–	–	–	–	–	3.87	4.21	2.16	1.79	–	–
Cr_2O_3	–	–	–	–	–	0.00	0.00	0.00	0.00	–	–

Sample	KEJ019	KEJ019	KEJ019	KEJ019	KEJ019	KEJ019	KEK019	KEJ019	KEJ019	KEJ019	KEJ019
Name	kej019mi22b	kej019mi22c	kej019mi23a	kej019mi23b	kej019mi23d	kej019mi21a	kej019mi21c	kej019mi21d	kej019mi19	kej019mi23c	kej019mi22d
Host	hbl	hbl	hbl	hbl	hbl	hbl	hbl	hbl	hbl	hbl	hbl
Period	2014	2014	2014	2014	2014	2014	2014	2014	2014	2014	2014
SiO_2	55.16	55.71	54.16	53.71	53.48	56.78	53.95	53.10	53.29	54.45	53.42
TiO_2	1.63	1.62	0.71	0.73	0.72	1.40	1.01	0.83	1.29	0.77	1.32
Al_2O_3	16.43	16.17	18.49	18.50	18.10	17.09	17.23	17.53	16.82	17.89	15.85
FeO	9.38	9.19	8.27	8.15	8.13	8.06	8.23	8.31	10.42	8.64	8.90
MnO	0.21	0.22	0.21	0.19	0.19	0.19	0.20	0.27	0.22	0.24	0.19
MgO	2.72	2.82	3.88	3.88	3.81	2.84	3.19	3.56	3.29	3.63	2.41
CaO	5.68	5.98	8.03	8.16	7.72	5.62	6.46	7.78	6.36	7.60	6.35
Na_2O	4.14	4.25	3.49	3.69	4.14	4.21	4.40	3.44	4.20	3.89	3.87
K_2O	2.90	2.51	1.36	1.27	1.54	2.51	2.33	1.20	2.53	1.66	2.25
P_2O_5	0.41	0.32	0.18	0.15	0.15	0.30	0.20	0.13	0.19	0.15	0.27
SO_2	bdl	0.03	bdl	bdl	0.03	bdl	0.03	bdl	bdl	bdl	bdl
Cl	0.62	0.52	0.33	0.31	0.33	0.34	0.56	0.37	0.66	0.36	0.65
Cr_2O_3	bdl	bdl	bdl	bdl	bdl	bdl	bdl	bdl	bdl	bdl	bdl
H_2O	0.68	0.55	0.66	0.58	0.90	0.60	1.18	3.26	0.55	0.58	0.87
sd	0.02	0.01	0.01	0.02	0.02	0.02	0.03	0.07	0.01	0.01	0.02
CO_2	109	48	98	104	94	90	91	52	37	67	250
sd	63	41	96	81	18	51	21	9	14	15	108
P_{sat}	25	13	27	27	29	22	33	98	11	18	70
Total	99.96	99.89	99.81	99.33	99.25	99.96	98.97	99.82	99.84	99.87	96.37

Major elements (in wt%) determined by electron microprobe; H_2O (in wt%) and CO_2 (in ppm) measured by ion-microprobe; sd (standard deviation) calculated by full error propagation of counting statistics, instrument background and calibration working curve; P_{sat} (saturation pressure) in MPa using method of Ghiorso and Gualda (2015); Olivine hosted melt inclusion compositions recalculated using average $Kd_{FeTotal\text{-}Mg}$ value of 0.22 for Kick-'em-Jenny lavas of Sigurdsson and Shepherd (1974) for which Fe_2O_3 and FeO were analysed separately; ol, olivine; cpx, clinopyroxene; hbl, hornblende; bdl; below detection limit.

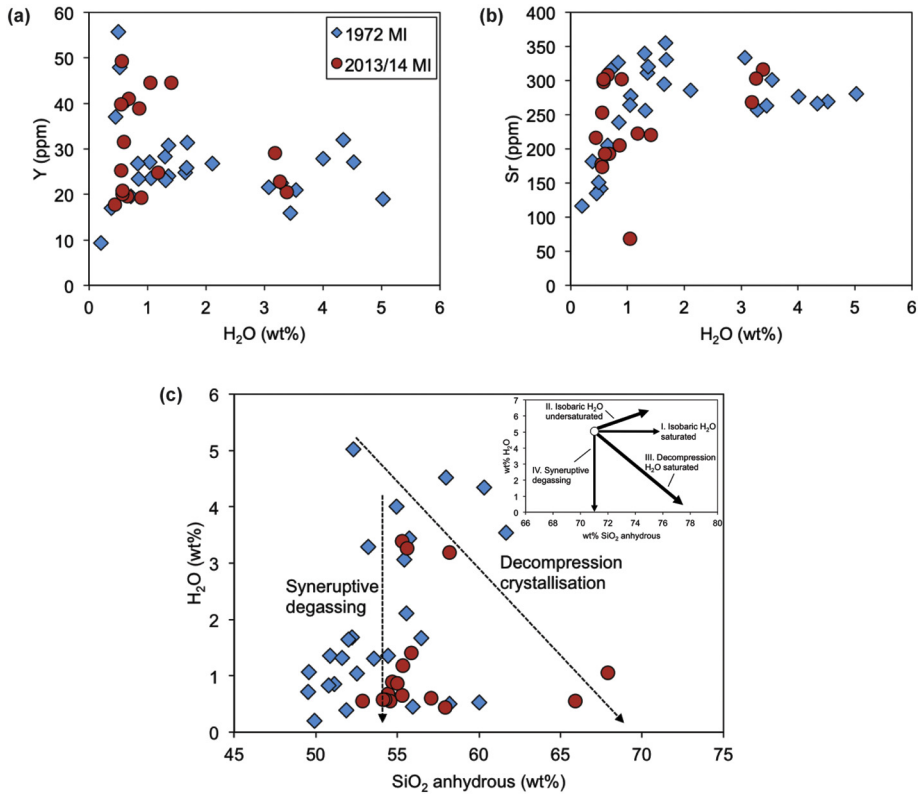

Fig. 10. Variation of selected trace elements (a) Y and (b) Sr with H_2O (all measured by SIMS) for Kick-'em-Jenny melt inclusions. (c) H_2O vs. SiO_2 (normalized to 100% H_2O free) plot. The dominant trends are consistent with decompression crystallisation (trend III) and syn-eruption degassing (trend IV) as displayed in the inserted schematic H_2O-SiO_2 plot showing trends anticipated for different crystallisation mechanisms after Blundy and Cashman (2005).

(964–968 °C) than for 2013/14 crater lavas (974–1055 °C) (Table 4, Fig. 11). Clinopyroxene-liquid thermometry for 1972 samples range 976–1008 °C, which is notably wider than temperatures obtained using hornblende-plagioclase calculations. 2013/14 landslide deposit basaltic andesite temperatures range 900–975 °C using hornblende-plagioclase and 969–1012 °C using clinopyroxene-orthopyroxene thermometers. The sole andesite (KEJ008a) ranges 820–840 °C using clinopyroxene-orthopyroxene. These distinctions are clearly represented in Fig. 11. Eruption temperatures using groundmass glass and olivine microlites range 1006–1022 °C for 1972 and 1079 °C for 2014 deposits. This matches well with extrapolated temperature estimates for microlite olivine (~1025–1050 °C) using the algorithm of Shejwalkar and Coogan (2013) (Fig. 5a). Kick-'em-Jack lavas range 946–1007 °C using hornblende-plagioclase phenocryst pairs.

Mean magma temperatures are notably low (~1000 ± 30 °C) for such magnesian lavas. However, the consistency of estimates for from the range of methods gives us confidence in our temperatures. The similarity of phenocryst and eruption temperatures is consistent with rapid ascent of magmas before eruption. We will return to the implications of this observation in a later section.

Table 4
Temperature estimates for Kick-'em-Jenny and Kick-'em-Jack volcanoes.

Volcano	Sample	T (°C)				
		hbl-plag	cpx-liq	cpx-opx	cpx-opx	ol-liq[a]
		Holland and Blundy (1994)	(Putirka, 2008)	(Putirka, 2008)	(Brey and Kohler, 1990)	(Putirka, 2008)
Kick-'em-Jenny	KEJ018 (1972)	964	–	–	–	1022
	KEJ005 (1972)	966	–	–	–	1023
	KEJ010 (1972)	968	976–1008	–	–	1006
	KEJ009 (1972)	–	1008	–	–	–
	KEJ014	990–1010	–	–	–	–
	KEJ019	983	–	–	–	1079
	KEJ008	977–1055	–	–	–	–
	KEJ048	974	–	–	–	–
	KEJ021	989	–	–	–	–
	KEJ032[b]	920-945	–	969-991	981–1012	–
	KEJ031[b]	900-975	–	973-986	983–1002	–
	KEJ008a[b]	–	–	840	820	–
Kick-'em-Jack	KEJ082	987	–	–	–	–
	KEJ086	946–1007	–	–	–	–
	KEJ084	955	–	–	–	–
	KEJ085	997	–	–	–	–

[a] Microlite-glass data.
[b] 2013/14 landslide deposits.

3.5.2. Magma storage pressures

Pressures were estimated by applying the MagmaSat solubility model of Ghiorso and Gualda (2015) to H_2O and CO_2 contents from phenocryst MIs assuming volatile saturation (Fig. 12). H_2O and CO_2 concentrations in MIs and volatile saturation pressure isobars for a median MI composition are plotted in Fig. 12a. A degassing trend is observed from high to low volatile contents. Magma storage pressures for Kick-'em-Jenny range up to 552 MPa, but the majority reach 325 MPa (Fig. 12b, Table 3). Highest pressures were obtained from melt inclusions containing high CO_2 (2500–3200 ppm) with correspondingly low H_2O (0.6–1.4 wt%) contents. We view these analyses with caution given the possibility that they may result from post-entrapment H_2O-loss, although we cannot rule out fluxing of previously degassed magmas by CO_2-rich fluids (Caricchi et al., 2018).

3.5.3. Oxygen fugacity

In the absence of appropriate oxybarometers to calculate the oxygen fugacity of Kick-'em-Jenny lavas, we apply the algorithm of Kress and Carmichael (1991) to eleven 1972 whole-rock samples from Sigurdsson and Shepherd (1974) who provide measured FeO/Fe_2O_3 ratio from which we can compute the fO_2 corresponding to Fe-redox equilibrium at P and T. The mean Fe^{3+}/Fe^{Total} for these samples is 0.28 ± 0.03, with no clear dependence on MgO. Using P = 300 MPa and T = 950 °C, fO_2 estimates for eleven 1972 basalts are in the range NNO +0.5 to +1.4 log units (with a single exception at NNO +0.05).

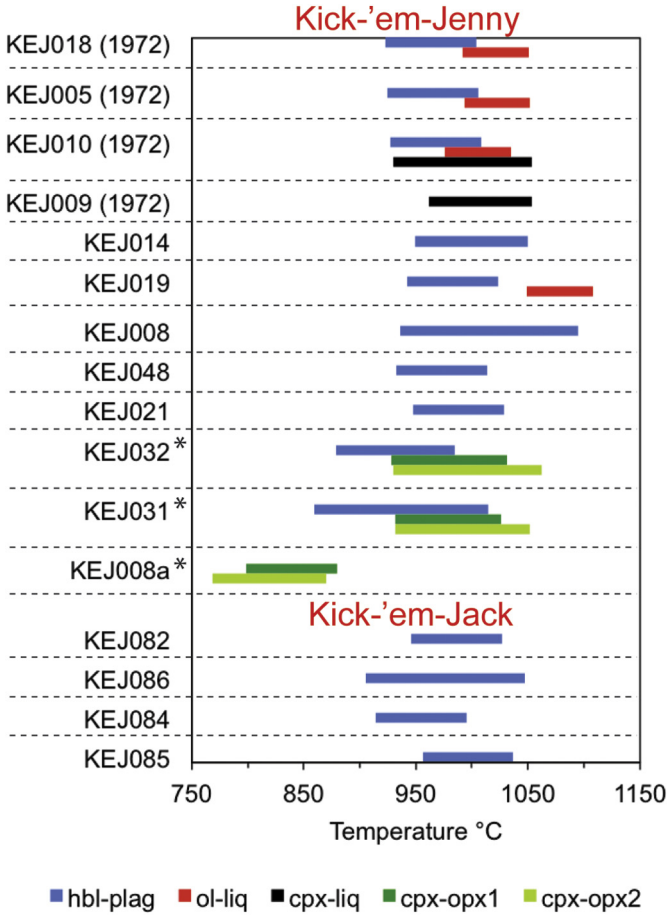

Fig. 11. Temperature estimates for Kick-'em-Jenny and Kick-'em-Jack lavas. Temperature ranges include errors associated with thermometers. Landslide deposits for 2013/14 Kick-'em-Jenny samples are given the symbol *. Thermometers used: hbl-plag, Holland and Blundy (1994) (±40 °C); ol-liq, Putirka (2008) (±29 °C); cpx-liq, Putirka (2008) (±45 °C); cpx-opx1, Putirka (2008) (±40 °C); cpx-opx2, Brey and Kohler (1990) (±50 °C).

4. Discussion

4.1. Crystal cargo origins

Crystal populations in Kick-'em-Jenny lavas contain phase assemblages and textures that suggest a complex magmatic history, including both changes in intensive variables during crystallisation and incorporation of xenocryst or antecryst material. Some melt inclusions (MIs) have compositions that overlap with Kick-'em-Jenny whole rocks, although most MIs are displaced from the whole-rock trend suggesting a change in crystallisation assemblage. Kinks in major element whole rock trends for CaO and Al_2O_3 (Fig. 8) also suggest changes in the crystallisation assemblage. Inferring the relative order of crystallisation for each phenocryst phase from included and excluded phases consequently proved problematic. Magnetite-rich (and Cr-rich when present) spinels are included in all phases suggesting they were the first to crystallise. Olivine grains only contained spinel inclusions suggesting they crystallised afterward. Clinopyroxene contained inclusions of spinel, olivine and plagioclase and showed replacement to hornblende. Hornblende contained inclusions of olivine, clinopyroxene and plagioclase, while some plagioclase grains also contained inclusions of hornblende. Although the olivines and spinels were demonstrably the first phases to crystallise there is therefore some ambiguity in the subsequent order of crystallisation of phases. It appears that a population of plagioclase grains (An_{96-79}) crystallised before clinopyroxene. After subsequent hornblende crystallisation, another population of plagioclase grains crystallised. The groundmass assemblage of olivine (Fo_{66-59}) + clinopyroxene = plagioclase (An_{79-46}) clearly formed outside the hornblende stability field. An obvious question is at what depth in the crust each population crystallised before eruption and whether crystals are primocrysts, antecrysts or xenocrysts.

The grain size arrangements, assemblages and textures of glomerocrysts are strikingly similar to the textures observed in cumulate crustal xenoliths brought to the surface by explosive eruptions in nearby Bequia (Camejo-Harry et al., 2018) and elsewhere in the Lesser Antilles (Cooper et al., 2016; Melekhova et al., 2017; Stamper et al., 2014a; Tollan et al., 2011). This supports the proposal that glomerocrysts may be either extracts of cumulate residues or lower pressure accumulations of near-liquidus minerals from H_2O saturated magmas that were incorporated following destabilisation of crystal mushes in the trans-crustal magmatic system (Camejo-Harry et al., 2018). The compositional similarity between glomerocrysts and phenocrysts suggests that a large proportion of phenocrysts may form by glomerocryst disaggregation. The large grain sizes (>2 mm) of various textural types of clinopyroxene, plagioclase and hornblende are indicative of a complex history. Lower degrees of undercooling would facilitate the slow growth of larger sized phenocrysts. Entrainment from the lower crust and subsequent transport to upper storage regions, reheating and possibly magma mixing would result in both reverse and normal zoning, sieve textures, reaction rims and resorption as the crystal cargo attempted to re-equilibrate to changing pressure (±temperature) during magma ascent.

At least three populations of isolated plagioclase phenocrysts clearly distinguished by grain size and An content, can be related to early and late plagioclase crystallisation. Large sized plagioclase phenocrysts (≥2 mm) containing zoning patterns of sizeable homogenous cores (An_{94-89}) with thin rims suggests conditions of crystallisation under conditions of low undercooling up until just before eruption, upon which conditions changed abruptly causing the crystallisation of compositionally different rims. Core crystallisation is likely to have occurred in deeper storage regions under near isobaric conditions over long time scales. Decompression-triggered crystallisation is a comparatively rapid process that promotes the crystallisation of small-sized plagioclases (<500 μm, An_{89-64}). Such crystallisation would have occurred as magmas ascended to shallow levels within the crust (<~100 MPa), which is supported by the MI trace (Fig. 10b) and major element (Fig. 10c) signatures. The associated drop in pressure causes water to

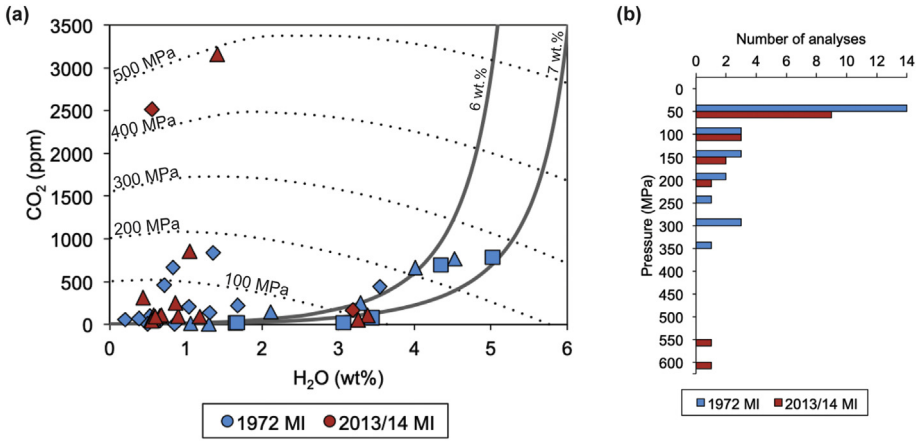

Fig. 12. (a) Volatile concentrations of CO_2 and H_2O in Kick-'em-Jenny melt inclusions. Isobars calculated using the MagmaSat solubility model (Ghiorso and Gualda, 2015) with a median melt inclusion composition and 950 °C. Melt inclusion hosts denoted as follows: diamond, olivine; square, clinopyroxene; triangle, hornblende. Vapour isopleths inserted as grey lines showing degassing trends for: (i) the most primitive rock composition (KEJ010 obtained from Devine and Sigurdsson (1995)) modelled to have originally contained 6 wt% H_2O (labeled) and 1.5 wt% CO_2 in the vapour and (ii) the melt inclusion with the highest measured H_2O content modelled to have originally contained 7 wt% H_2O (labeled) and 1.5 wt% CO_2 in the vapour. (b) Melt inclusion entrapment pressures for a given analysis.

exsolve providing the undercooling that drives crystallisation. Other plagioclase grains (ranging >500 μm and <2 mm) exhibited oscillatory zoning and abundant sieve textures possibly obtained from fluctuating conditions resulting from reheating of shallower magmas by hotter deeper magmas and decreasing water pressures as phenocrysts grew en route from mid crustal storage regions to shallow levels.

Hornblende is uncommon as a phenocryst phase in basic rocks because of its instability at low pressures in basaltic magmas (Rutherford and Hill, 1993) and the increased crystallinity that often accompanies hornblende crystallisation from hydrous basalts which results in increased magma viscosity and reduced eruptability (Barclay and Carmichael, 2004). Its prevalence in Kick-'em-Jenny lavas suggests that magma transit through the crust from deep magma storage regions kept pace with the slope of the hornblende-in curve, enabling it to remain saturated over a wide pressure range (Allen and Boettcher, 1983). Eruption would have had to be sufficiently rapid to prevent complete hornblende resorption. The calculated hornblende-plagioclase temperatures are in good agreement with the coexistence of these two minerals according to the water-undersaturated experiments of Holloway and Burnham (1972) (975 °C, 250 MPa). For water-saturated conditions, hornblende and plagioclase are found to coexist only at 1000 °C, 50 MPa (Barclay and Carmichael, 2004).

In summary, we propose on the basis of crystal textures and complex crystallisation sequences that the Kick-'em-Jenny and Kick-'em-Jack crystal cargos could have resulted from polybaric crystallisation of magma batches as they ascend through the crust and interact. In such a situation the different slopes of crystal saturation curves for a hydrous basalt and the exact P-T trajectory followed during ascent can give rise to very complex zonation patterns. In this regard the presence of early crystallising Fo-rich olivine and late crystallising groundmass olivine is striking.

4.2. A case for cold, primitive, wet basalts

Kick-'em-Jenny has erupted some unusually MgO-rich magmas (≤13 wt%), raising the possibility that these are truly primitive, mantle-derived melts. Alternatively, the magnesian character of Kick-'em-Jenny magmas might simply correspond to large amounts of accumulated antecrystic or xenocrystic material. A number of chemical and petrographic criteria can be used to distinguish between these possibilities.

Xenocryst (or antecryst) addition would be expected to lead to correlations between xenocryst proportions and bulk rock chemistry. For example, if mafic phenocrysts are xenocrystic, we would expect the most magnesian lavas to have the highest modal proportions. This is observed for hornblende phenocrysts, leading previous authors to conclude that hornblende assimilation is an important process occurring beneath Kick-'em-Jenny (Devine and Sigurdsson, 1995). However, the extent of hornblende addition observed cannot adequately account for the major element chemistry of Kick-'em-Jenny basalts as the hornblende phenocrysts in basalts contain only 14.7 wt% MgO, on average (Supplementary Table S1e), a value only slightly greater than that of the basalts themselves. Moreover, the low Ni and Cr contents of hornblendes cannot drive basalts to the observed levels that are, instead, consistent with values for mantle-derived magmas. Addition of xenocrystic hornblende should to lead to a reduction in incompatible trace element concentrations, e.g. for Zr, Rb and Ba, which do not occur in hornblende to a significant degree. Passmore et al. (2012) used similar arguments to assess xenocryst incorporation in porphyritic Icelandic lavas. At Kick-'em-Jenny we see no negative correlation between modal hornblende and incompatible trace element concentrations (Supplementary Fig. S3).

Finally, xenocryst incorporation would be expected to yield discrete overgrowth or resorption textures around xenocryst cores. Although some olivines have magnesian cores with abrupt overgrowths (Fig. 4c), most large phenocrysts of hornblende and clinopyroxene display complex zonation patterns, consistent with primocrysts that are attempting to keep pace with changing pressure and temperature during magma ascent. This is likely to be especially important for hornblende due to its upper temperature stability limit of ≤1100 °C in basaltic magmas (Fig. 4, Melekhova et al., 2015). Magmas that ascend at or close to this temperature will tend to graze the hornblende liquidus leading to abrupt changes in stability and modal proportion, resulting in complex zonation patterns. These lines of evidence lead us to the conclusion that the magnesian character of Kick-'em-Jenny lavas is not simply a product of hornblende (or other xenocryst) assimilation.

If Kick-'em-Jenny lava chemistry is not controlled by crystal accumulation, then it must reflect either differentiation of a parental primitive magma or represent a range of primitive compositions, i.e. a range of magmas consistent with derivation from a peridotitic mantle source. The presence of rare $Fo_{\geq 90}$ olivine cores is consistent with such a scenario. We can calculate the Fo content of olivine in equilibrium with Kick-'em-Jenny magnesian lavas using $Kd_{FeTotal\text{-}Mg}$ $(=[Fe^{Total}/Mg]_{ol}/[Fe^{Total}/Mg]_{melt})$. The presence of significant ferric iron needs also to be taken into account. Assuming that Fe^{3+} does not enter the olivine structure, the apparent $Kd_{FeTotal\text{-}Mg}$ will be reduced from the canonical value of 0.31 in proportion to the amount of ferric iron, i.e. $Kd_{FeTotal\text{-}Mg} = 0.31 * (1 - Fe^{3+}/Fe^{Total})$. As noted above, for the eleven Kick-'em-Jenny lavas of Sigurdsson and

Shepherd (1974) for which Fe_2O_3 and FeO were analysed separately, calculated $Kd_{FeTotal-Mg}$ values are in the range 0.21 to 0.24 and the calculated equilibrium olivine compositions range from Fo_{91} to Fo_{78}. For typical mantle with primary (unreacted) Fo_{92-89} olivine, as recorded by mantle xenoliths from nearby Grenada (Parkinson et al., 2003), these calculations indicate that all Kick-'em-Jenny lavas with ≥8 wt% MgO are plausibly primitive, i.e. in equilibrium with mantle peridotite. On this basis, we suggest that all Kick-'em-Jenny lavas more magnesian than this represent primitive magmas. Their chemical variation can be ascribed to differing melting conditions and source mineralogy, for example, in terms of the amount of hornblende initially present at the onset of melting. Conversely, magmas with <8 wt% MgO reflect distinct chemical differentiation trends that can be ascribed to crystallisation of the observed phenocryst assemblages, notably hornblende which serves to drive down both CaO and MgO. The continued increase in Al_2O_3 below 8 wt% MgO (Fig. 8) indicates that the proportion of fractionating plagioclase must be minor, despite its relative abundance as a phenocryst.

The relatively low calculated phenocryst and eruption temperatures (1000 ± 30 °C) reported above, coupled with high H_2O contents (≤5 wt %), of Kick-'em-Jenny lavas provide clues as to their mantle origins. For magmas that ascend rapidly through the crust, as suggested by the preservation of the hornblende phenocrysts, magma source and eruption temperatures are expected to differ only by the combination of adiabatic cooling (~50 °C/GPa; Carmichael (2002)) and release of latent heat of crystallisation (~2.5 °C per % crystallised; Blundy et al. (2006)). As these effects broadly cancel out in the case of Kick-'em-Jenny, we infer that the source melting temperatures for primitive basalts (>8 wt % MgO) was of the order 1000 °C. This is strikingly similar to the dehydration melting solidus of hornblende-peridotite. According to the experimental data of Niida and Green (1999), the volatile-absent, hornblende-lherzolite solidus ranges from 980 °C at 0.8 GPa to 1000 °C at 1.5 GPa. Under these conditions, near-solidus melts would be H_2O-rich and magnesian, although, to date, no experimental studies of hornblende-peridotite melting have reported glass compositions. It is noteworthy that the melting interval over which hornblende (pargasite) and melt coexist during melting is around 30 °C. Over this interval melt composition is expected to change significantly because of the incongruent nature of pargasite melting (Niida and Green, 1999). Thus chemical variation in primitive melts may result from isobaric melting in the presence of hornblende beneath Kick-'em-Jenny. The curious kink in whole rock CaO contents around 8–10 wt% MgO (Fig. 8) may reflect such source controls on basalt chemistry.

Melting of mantle peridotite with various modal proportions of hornblende can provide a plausible interpretation of Kick-'em-Jenny magnesian basalts. However, phenocryst temperature calculations for basalts (1972) are somewhat lower (964–1008 °C, Table 4 & Fig. 11) than groundmass (eruption) temperatures (1006–1023 °C). We attribute this difference to the effects of adiabatic cooling and latent heat of crystallisation, whose combined effect is very little change in temperature from source to surface. The exact P-T trajectory that ascending basalts will follow depends on the relative rates of ascent and crystallisation. At Kick-'em-Jenny we suggest that adiabatic cooling preceded significant crystallisation, giving rise to phenocryst temperatures that are slightly lower than eruption temperatures.

A primary origin for magnesian Kick-'em-Jenny basalts is consistent with the presence of primitive basalts on Grenada to the south and St. Vincent (Bouvier et al., 2008; Heath et al., 1998) to the north. However, the nature of those primitive basalts and the melting processes that generated them are very different from those inferred for Kick-'em-Jenny. For example primary basalts on St. Vincent are thought to derive from partial melting of peridotite at 1130 to 1180 °C in equilibrium with a hornblende-free residuum (Heath et al., 1998) at pressures of ~1.4 GPa according to the multiple saturation experiments of Pichavant et al. (2002) and Melekhova et al. (2015). These conditions are more typical of primitive arc basalts worldwide with eruption temperatures ~1160 to 1200 °C (Tatsumi and Eggins, 1995). The mantle source depth of primitive Grenada basalts is less clear, although their rare earth element chemistry (Shimizu and Arculus, 1975) and high eruption temperatures (ol + cpx + spl one atmosphere liquidus = 1325 °C; Stamper et al. (2014a)) argue for a deep, garnet-bearing peridotite source, again markedly different for the source conditions of Kick-'em-Jenny hornblende basalts. The geographical proximity of Kick-'em-Jenny to Grenada (8 km apart) makes the difference in mantle source regions intriguing, perhaps reflecting the local structure and mineralogy of the sub-arc mantle and slab.

4.3. Fate of dissolved volatiles

High concentrations of H_2O were measured in Kick-'em-Jenny magmas (up to 5.0 wt%), consistent with the striking abundance of hornblende in erupted lavas together with delayed plagioclase crystallisation. High Al_2O_3 contents of hornblendes also suggest crystallisation at high H_2O pressure (Grove et al., 2003; Melekhova et al., 2015; Nandedkar et al., 2014; Pichavant and Macdonald, 2007; Sisson and Grove, 1993). Fig. 12a confirms that H_2O-rich conditions correspond to greater pressures (and hence depths) within the crust than H_2O-poor conditions, a consequence of decompression-driven degassing, rather than isobaric, volatile-saturated crystallisation. Trace element geochemistry of MIs clearly demonstrates the proclivity of plagioclase crystallisation for lower pressure, H_2O poor conditions (Fig. 10b). Strontium, as a proxy for plagioclase crystallisation, shows high concentrations in the melt at high H_2O contents where plagioclase crystallisation is hindered, and a decrease in Sr concentrations as H_2O contents decrease enough for plagioclase to crystallise. Such plagioclase crystallisation would have been facilitated by decompression, accompanied by H_2O loss (Fig. 10c) and may also account for the increase in incompatible elements with decreasing H_2O (Fig. 10a). Of the remaining trace elements measured, only yttrium is significantly compatible in hornblende and likely to be taken up within its crystal structure during crystallisation at higher H_2O contents. As water concentrations decrease, hornblende becomes unstable and begins to break down, and elements such as Y are returned to the melt, plausibly accounting for its enrichment at low H_2O contents (Fig. 10a). The fact that many MIs preserve decompression crystallisation signals suggests that these MIs maintain some connection with the matrix glass after incorporation in the host mineral, as previously suggested by Blundy and Cashman (2005) for silicic MIs from Mount St. Helens.

Although magmas lose their dissolved volatiles as a natural consequence of ascent and eruption (Metrich and Wallace, 2008), knowledge of the initial water content of magmas is important since it can affect various aspects of magmatic evolution from source to eruption. MIs trapped in the earliest forming crystals stand the best chance of preserving original H_2O concentrations (Plank et al., 2013; Wade et al., 2008; Zimmer et al., 2010). Such crystals would usually be olivine, but at Kick-'em-Jenny the MI with the highest measured water content (5 wt%) was hosted in clinopyroxene, while olivine-hosted MIs contain <3 wt% H_2O (Fig. 12a). There are no MIs preserved in the Fo_{90} olivines thought to represent the deepest crystallisation conditions. The observed H_2O range is appreciably lower than would be expected for dehydration melts of hornblende-peridotite, estimated to be on the order 10–12 wt% by Niida and Green (1999). If Kick-'em-Jenny basalts were indeed derived by hornblende-peridotite melting then the actual water (and potentially CO_2) content would be significantly higher than 5 wt%. In that case, either MIs have lost their original H_2O upon stalling in upper crustal reservoirs causing inclusions to reset to lower H_2O concentrations (Bucholz et al., 2013) or their host minerals crystallised at lower pressures during magma ascent. Blundy et al. (2010) have shown that decompression crystallisation can lead to MIs trapping after a significant fraction of the original magmatic volatile content has been exsolved for the case where the initial dissolved CO_2 content was relatively high. In this case, both the H_2O and CO_2 contents

of Kick-'em-Jenny primitive magmas may have been considerably higher than those recorded by MI trapped during decompression crystallisation of olivine and clinopyroxene within the crust. In that case, the high CO_2 contents of some MIs might be an indication of the original magmatic contents, albeit their low H_2O contents must have been significantly modified by diffusive processes, e.g. Bucholz et al. (2013).

The generally low CO_2 contents of Kick-'em-Jenny MIs points towards significant degassing on magma ascent. The degassing paths taken by MIs with the highest volatile contents from high to low pressures within the crust (Fig. 12a) implies that the magmatic system is highly pressurised with respect to H_2O and CO_2 at depth. Using the MagmaSat model of Ghiorso and Gualda (2015), we can model the path a primitive melt from depth would have followed during depressurisation in a closed system. Using the most magnesian bulk rock composition for Kick-'em-Jenny lavas (1972 KEJ010, Devine and Sigurdsson (1995)), we can vary the initial H_2O and CO_2 content until the modelled degassing paths match our data. The best fit for our data using this composition requires magma to have been initially H_2O rich (6 wt%) and CO_2-rich (1.5 wt%), which is significantly higher than estimated from MIs (Fig. 12a), but still not as high as the primitive melt H_2O contents for dehydration melting of hornblende-peridotite proposed by Niida and Green (1999). A similar trend calculated through the MI with the highest measured H_2O content requires initially 7 wt% H_2O and 1.5 wt% CO_2 (Fig. 12a). CO_2-rich (2.5–3.2 wt%) MIs perhaps provide a rare glimpse of the deeper magmatic system (Fig. 12). Clearly further experimental studies of the major element composition and volatile contents of melts of hornblende-peridotite are required.

The presence of a volatile-charged system at depth beneath Kick-'em-Jenny has ramifications for hazard assessment especially if such volatiles are not periodically released and allowed to build up in the system. The fact that such high volatile contents were present in volcanic rocks (lavas) suggests that there must have been some mechanism for efficient outgassing to promote effusive behaviour. Dondin et al. (2017) propose that brittle deformation of the rocks making up Kick-'em-Jenny's edifice increases rock permeability allowing outgassing from magma reservoirs through fracture networks. Effusive behaviour will therefore be encouraged in lieu of explosive activity. These authors go on to suggest that explosive activity may be triggered by the presence of a low permeability lava dome capping the crater (which has been observed at this volcano in the past (Lindsay and Shepherd, 2005)) that can prevent the release of volatiles from the magmatic system. If the rate of magma ascent exceeds the rate of volatile release through fracture networks, explosive behaviour may also be favoured (Dondin et al., 2017).

4.4. Changes in Kick-'em-Jenny between 1972 & 2014: implications for hazards

Because sample collection for 1972 and 2013/14 expeditions occurred some years after the last preceding documented eruption (Table 1), we cannot say with absolute certainty that crater lavas are exclusively representative of those eruptions. Sigurdsson and Shepherd (1974) describe the 1972 collection as fresh and lacking associated organic material signifying the occurrence of eruptions between 1966 and 1972. The same may have occurred between the 2001-documented eruption and the 2013/14 expeditions. We therefore treat these sample collection dates as minimum eruption periods.

1972 and 2013/14 crater and cone lavas contain similar mineral assemblages, textures and chemistries. However, there are certain differences between the eruptive products from each time cohort that indicate an evolution in the volcanic system over 40+ years. Firstly, the erupted rock types have changed from predominantly basaltic in 1972 (Devine and Sigurdsson, 1995) to basaltic andesite in composition in 2013/14 (Supplementary Fig. S1). MI compositions also show a broader range in 2013/14 deposits from basaltic andesite to dacite while 1972 MIs span basalt to basaltic andesite. Thirdly, there is evidence for a reduction in the crystallisation temperatures of olivine. The Ca content of olivine has been shown to be primarily dependent on temperature in the presence of clinopyroxene (Shejwalkar and Coogan, 2013). The calculated isotherms using the algorithm of Shejwalkar and Coogan (2013) for orthopyroxene-bearing 2013/14 landslide deposits show that olivine crystallisation for Kick-'em-Jenny occurred over a temperature range of 900–1050 °C (Fig. 5b). As expected, compositional factors exercise some control on crystallisation temperatures, but what is more apparent is that some 2013/14 olivine crystallised under lower temperatures than 1972.

Omitting unusually high CO_2-low H_2O MIs, it is apparent that eruptions making up the 1972 sample collection derive from both deep and shallow magma storage regions, whereas the eruptions contributing to the 2013/14 samples tapped mainly the shallower reservoirs (Fig. 12b). This may have ramifications for flank stability at Kick-'em-Jenny. If recent eruptive activity is indeed concentrated at a shallower depth, the likelihood for a magmatic component triggering flank collapse is heightened. Even though an explosive eruption is unlikely to trigger a tsunami at the volcano's current elevation (Lindsay et al., 2005), shallow magma injection as a destabilising mechanism combined with the noted instability of the volcano's edifice (Allen et al., 2018; Dondin et al., 2017) increases its susceptibility for slope collapse which may trigger a tsunami.

We see a situation where the volcano's future eruptive compositions will likely become predominantly more silicic than previous eruptions as time progresses. The tendency for explosive or dome-forming eruptions, that may eventually lead to explosive eruptions as the permeability of the edifice is decreased, is also greater because of the accompanying increase in magma viscosity. If a significant episode of cone building does occur as a result of such compositional changes, the likelihood of a tsunami threat will be increased (Allen et al., 2018). The added complication of a shallow magma reservoir makes this volcano a prime candidate for multiple direct and indirect hazards to nearby populations on Grenada and the Grenadines.

4.5. Linking geochemical variations to Kick-'em-Jenny's structural history

All mineral phase (except clinopyroxene) and bulk rock compositions from Kick-'em-Jenny volcano display consistent differences between crater/cone deposits (irrespective of sampling period) and landslide deposits. Although Kick-'em-Jack samples are too few to adequately compare bulk rock compositions, hornblende compositions (Fig. 6) display a remarkable similarity to Kick-'em-Jenny landslide deposits. These variations agree with current understanding of the different incarnations of Kick-'em-Jenny volcano. The constraints on sample collection for 2013/14 crater deposits and their similarity to 1972 deposits suggest that these samples characterize the current edifice of Kick-'em-Jenny. The locations of 2013/14 landslide deposits (possibly including Kick-'em-Jack landslide deposit samples), combined with their geochemical similarities, imply that these samples may be older than crater deposits and may be in fact more related to the volcano's proto edifice.

Before delving into geochemical distinctions, the first key difference lies in mineral assemblages (Fig. 2): 1972 and 2013/14 crater/cone deposits contain assemblages of olivine, clinopyroxene, hornblende, plagioclase and spinel whereas 2013/14 landslide deposits also contain these phases but with minor olivine and the addition of orthopyroxene. More evolved Kick-'em-Jack landslide deposits are also different, containing only hornblende, plagioclase and spinel. Kick-'em-Jenny 1972 and 2013/14 crater deposits display a separate trend of higher CaO contents for a given MgO from 2013/14 landslide deposits (Fig. 8b). This is indicative of different pressures of crystallisation as modelled for the M- and C-series lavas of Grenada by Stamper et al. (2014b). Lower pressures delay the onset of clinopyroxene saturation relative to olivine (Stamper et al., 2014b); initial, protracted crystallisation of olivine

enriches the melt in CaO. The result is a differentiation path matching 1972 and 2013/14 crater deposits, although, these do not reach CaO contents as high as Grenada C-series. Higher pressures allow near simultaneous crystallisation of clinopyroxene and olivine, depleting the melt in both CaO and MgO and producing a trend matching 2013/14 landslide deposits, similar to that seen in Grenada's M-series, albeit starting at lower initial MgO. Al_2O_3 contents suggest that H_2O contents were higher, and plagioclase crystallisation was later, in melts producing crater deposits compared to landslide deposits (Fig. 8c). The absence of orthopyroxene in crater deposits may also be related to higher magmatic H_2O contents, which tends to stabilise olivine by reducing silica activity (Sisson and Grove, 1993). Hornblende-plagioclase crystallisation temperatures are comparatively lower in landslide deposits than crater deposits (Table 4).

We propose that 2013/14 landslide deposits were generated from melts originating at higher pressures than 1972 and 2013/14 crater deposits. Plagioclase crystallisation occurred later in crater than landslide deposits, possibly aided by higher H_2O contents. If landslide deposits are indeed representative of Kick-'em-Jenny's proto edifice, there appears to have been an upward migration in the depth of melt generation with this new incarnation of the current edifice. In many cases, Kick-'em-Jack landslide deposits match Kick-'em-Jenny landslide deposits, however, the limited bulk rock data are equivocal, showing similarity to the crater deposit trend or lying in between two trends (Figs. 8 & 9). It is very likely that Kick-'em-Jack landslide deposits are related to Kick-'em-Jenny deposits, but represent more evolved samples from an older Kick-'em-Jack edifice (plausibly proto Kick-'em-Jenny).

4.6. Kick-'em-Jenny plumbing system

Measurements of dissolved volatiles in MIs provide only a minimum estimate of magma storage pressures if the melts were not volatile-saturated at the point of entrapment (Blundy and Cashman, 2008) or if significant degassing preceded MI trapping (Blundy et al., 2010). Pressures (Fig. 12b) can be converted to depths using an appropriate density model (2750 kg/m^3 for ≥250 MPa and 2500 kg/m^3 for MI <250 MPa). On the basis of MI volatile saturation pressures, we propose that Kick-'em-Jenny's crustal magmatic system consists of a main reservoir somewhere between 7 and 12 km depth (Fig. 13), with shallower networks of smaller melt lenses and crystal mushes interconnected by sub-vertical feeding structures. Rare CO_2-rich MIs contain low H_2O contents that suggest the interaction between stalled magma and ascending CO_2-rich vapours originating deep within the plumbing system. Evidence that this magmatic system extends throughout the crust comes also from hypocenters of pre-eruptive earthquakes collected from the 2015 and 2017 eruptions (obtained from UWI-SRC) that cover a similar depth range (Fig. 13).

As for other arc systems, mantle-derived basalts are injected into the lower crust, upon which fractionation occurs forming cumulate piles and residual melts. For Kick-'em-Jenny, the temperature of melts coming out of the mantle, on the basis of the phenocryst and eruption thermometry results presented above, are unusually low (~1000 °C) given the Mg-rich nature of the least evolved basalts. Hydrous mantle melts can be generated from hornblende-peridotite sources at these temperatures via dehydration melting at pressures of around 1 GPa. These low temperatures promote hornblende stability in primitive basaltic melts and their derivatives, in contrast to much hotter primitive magmas from St. Vincent and Grenada. Because mantle melting involves incongruent breakdown of hornblende (Niida and Green, 1999), melts of hornblende-peridotite are likely to be enriched in hornblende components. In fact, as noted above, the bulk composition of the most primitive Kick-'em-Jenny lavas are quite similar to their hornblende phenocrysts. Because melts produced from hornblende-peridotite will have a high dissolved hornblende content they are likely to crystallise copious quantities of hornblende during ascent, provided that temperatures during ascent lie within the hornblende stability field. There are no phase equilibrium studies of Kick-'em-Jenny basalts, but studies of a tholeiitic basalt in equilibrium with a mixed H_2O-CO_2 fluid ($XH_2O = 0.59$) over a wide pressure range (Holloway and Burnham, 1972) show that the hornblende-in curve has a slope of ~125 °C/GPa in the pressure range 0.8 (1050 °C) to 0.2 (975 °C) GPa; below 0.2 GPa the hornblende liquidus curves sharply to much lower temperatures, reflecting its instability at low pressure. We suspect that the XH_2O in the source region of Kick-'em-Jenny primitive basalts was somewhat greater than that of 0.59, leading to slightly lower hornblende liquidus temperatures. For example, for the H_2O-saturated case, hornblende saturation temperatures are around 40 °C lower, but the corresponding slope on the hornblende-in curve is ~133 °C/GPa, i.e. 0.8 GPa, 1010 °C and 0.2 GPa and 930 °C (Krawczynski et al., 2012). Thus, near adiabatic ascent of primitive Kick-'em-Jenny basalts is likely to track the hornblende liquidus, producing hornblende crystals over a very broad pressure interval (Fig. 13). Olivine of contrasting Fo content will bracket hornblende crystallisation, from Fo_{90} close to the mantle source region to $Fo_{70–60}$ in lower pressure microlites and crystal rims, following significant hornblende and clinopyroxene crystallisation. We suggest that this accounts for large size of Kick-'em-Jenny and Kick-'em-Jack hornblende phenocrysts and their complex zoning, as well as providing constraints on the ascent path of these magmas.

Primitive magmas ascend to feed middle and upper crustal reservoirs and in doing so become increasingly chemically evolved. This process may involve classic crystal fractionation, whereby melts and crystal become separated from each other, closed system crystallisation, or entrainment of crystal cargos from the surrounding lithologies. Crystal cargos are plausibly dominated by mafic phases at depth that are progressively replaced by felsic phases with decreasing vertical depth. Upper crustal reservoirs are likely sustained by the destabilisation of ponded magma in the mid-crust (Cashman et al., 2017) which may be initiated by diverse melts percolating the mush effectively driving fluctuating conditions of the system and maintaining instability. Magmas with >8 wt% MgO are considered to be diverse primitive melts from hornblende-bearing peridotite sources in the sub-Kick-'em-Jenny mantle. The diversity in melts with <8 wt% MgO (Table 3) may be due to fractional crystallisation, but might equally represent a range of primitive melts with different evolutionary histories and water contents that are allowed to percolate crystal mushes beneath Kick-'em-Jenny. Reversely zoned phases suggest the infiltration of hotter melts forming high temperature rims within magma reservoirs already containing more evolved melts. These varied compositions encourage the mixing of magma batches (for which we have seen evidence, Fig. 3f) allowing cumulates, glomerocrysts and antecrysts to be entrained and transported to different storage regions and eventually erupted in lava flows. The amount of volatiles contained will be determined by their initial abundance in mantle-derived basalts, which may become enriched upon magma differentiation and evolution. Magma ascent and later decompression in lower storage regions will cause volatile exsolution thereby increasing the bubble content of the magma.

The high initial volatile contents and highly pressurised, vertically extensive system beneath Kick-'em-Jenny make it plausible that volcanic eruptions may be driven by deeply generated volatiles, as proposed for Soufrière Hills, Montserrat, by Christopher et al. (2015). Increased magma pressure together with the mixing of diverse melts can lead to a major destabilisation of the trans-crustal magmatic system, which in turn can provide the overpressure required for an eruption. Periods of dormancy between eruptions are marked by a return of the system to a period of relative stability where the major fluxes are caused by basalt injection at depth which slowly evolves by the fractionation of segregated melts. As melt layers begin to connect and move upward in the system, more silicic magma are disrupted allowing volatiles to be liberated and magma pressure to be increased, returning the system to a period of unrest (Christopher et al., 2015).

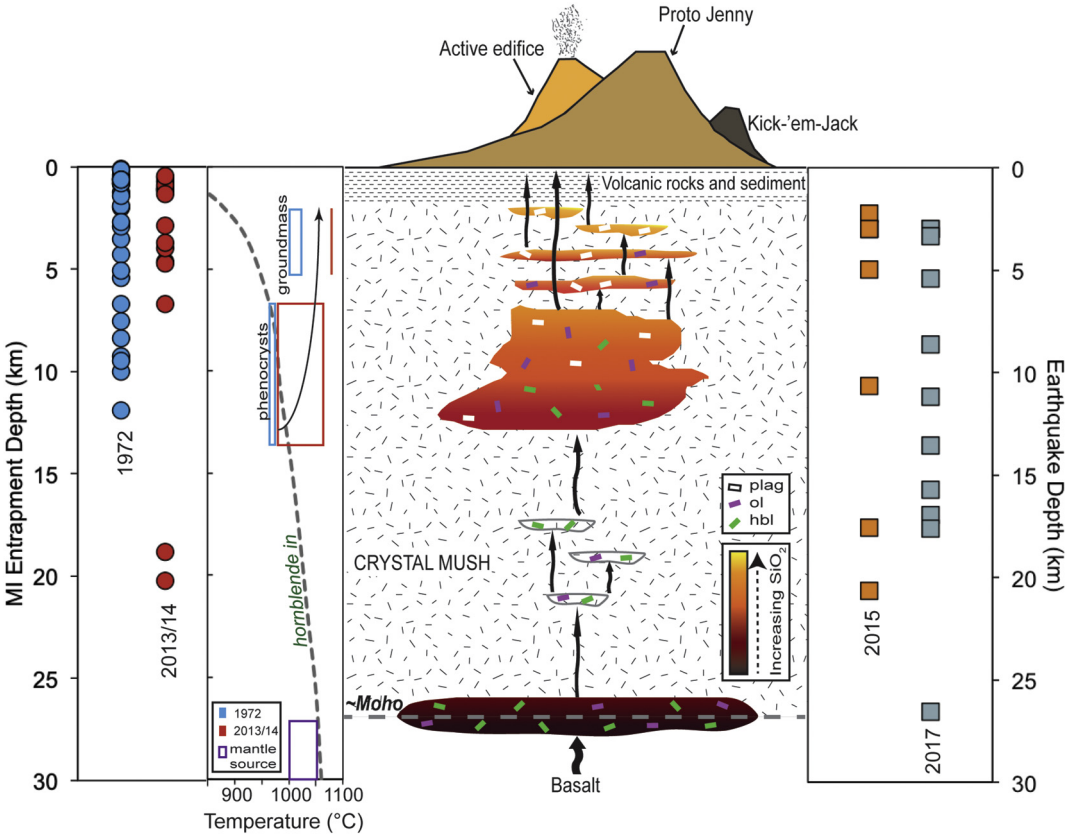

Fig. 13. Schematic illustration of the sub-volcanic system beneath Kick-'em-Jenny volcano. The system is composed of a chief magma storage region (~7–12 km) and shallower reservoirs all connected by sub-vertical feeding structures. Shown on the left are entrapment depths for 1972 and 2013/14 phenocryst hosted melt inclusions. Density models used: 2750 kg/m^3 for melt inclusions trapped at ≥250 MPa and 2500 kg/m^3 for melt inclusions trapped at <250 MPa. The adjacent panel displays calculated olivine-liquid and hornblende-plagioclase thermometry for groundmass and phenocrysts respectively, temperature range for mantle source region of basalts and the inferred hornblende-in curve after Holloway and Burnham (1972). The arrow denotes inferred magma ascent P-T trajectory. Shown on the right are pre-eruptive earthquake depths for 2015 and 2017 eruptions. Errors on these depths are ± 10 km. Pre-eruptive events occurred July 12–22, 2015 and July 8–28, 2017 respectively (monitoring data provided by the UWI-SRC database). The Moho is placed at 27 km after Christeson et al. (2008). Mantle-derived hydrous basalts are injected at depth upon which fractionation and migration of residual melts to upper storage regions occurs. Melt compositions can be varied as denoted by SiO_2 content. At depths greater, melt lenses are inferred by grey polygons. With decreasing depths, crystal cargos and residual melts become progressively evolved.

5. Conclusion

Kick-'em-Jenny volcano has erupted basalts, basaltic andesites and andesites with glomeroporphyritic textures. Phenocryst phases differ according to the location of sample collection: crater deposits contain spinel, olivine, clinopyroxene, hornblende and plagioclase while landslide deposits contain similar phases with comparatively less olivine and the addition of orthopyroxene. Evidence for disequilibria such as zoning, breakdown rims and sieve and replacement textures are recurring features of phenocrysts. The H_2O content of Kick-'em-Jenny magmas, as measured from melt inclusions (MIs), is ≤5 wt%, but may be significantly higher if MIs were trapped after significant ascent and degassing. Crystallisation temperatures, from a variety of thermometers, are surprisingly low for such MgO-rich basalts (~1000 °C). The high H_2O concentration and low temperature explains the abundance of hornblende phenocrysts as well as high Al_2O_3 contents and corresponding delayed plagioclase crystallisation. The presence of Fo_{90} olivine phenocryst cores, MgO- and Ni-rich whole rock chemistry, and low eruption temperatures of Kick-'em-Jenny basalts is consistent with a mantle source of hornblende-peridotite that undergoes dehydration melting.

A comparison of 1972 and 2013/14 crater samples shows an evolution in erupted deposits from predominantly basaltic to basaltic andesite in composition. MI compositions have also expanded in range from basaltic to andesitic to basaltic andesite to dacitic in more recent eruptions. MI data provide evidence for a highly pressurised, vertically extensive magma system originating in the mantle wedge but with a principal magma storage region ~7–12 km. This has implications for the type of eruptive activity expected especially if gases are not periodically exsolved from the magmatic system. The fact that such high volatile contents were measured in extrusive rocks suggests there is currently some mechanism for efficient outgassing to promote effusive behaviour. It is likely that this temporal compositional evolution of Kick-'em-Jenny magmas will have a control on the nature of future eruptions.

The spatial differences in sample collection have also revealed distinctions in rock and mineral geochemistry. We have used this to show that crater deposits from 1972 and 2013/14 sample Kick-'em-Jenny's current edifice, while 2013/14 landslide deposits likely represent proto Kick-'em-Jenny (an edifice existing pre 43.5 kyr BP). 2013 Kick-'em-Jack landslide deposits are also likely related to proto Kick-'em-Jenny substantiating previous suggestions that these volcanoes may belong to the same volcanic complex. The magmatic systems beneath these two incarnations of Kick-'em-Jenny have also changed over time, with the depth of melt generation decreasing and melt H_2O content increasing between these periods.

Supplementary data to this article can be found online at https://doi.org/10.1016/j.jvolgeores.2019.01.023.

Data access statement

All underlying data are provided in full within this paper, either in the main text or as accompanying supplementary material.

Acknowledgments

This research was supported by a Commonwealth Scholarship to MC-H, funded by the UK Government and a Natural Environment Research Council (NERC) grant NE/N001966/1; United Kingdom (UK) Government to EM and JB. We thank Stuart Kearns for help with EPMA, Richard Hinton for assistance with SIMS and Jenni Barclay for facilitating XRF analysis. We recognize the National Science Foundation grant OCE-1258771, which provides support for the curation and distributions of geological samples at the University of Rhode Island. We thank Lucy McGee and an anonymous reviewer for their comments and suggestions that improved the manuscript and James Gardner for editorial handling.

References

Allen, J.C., Boettcher, A.L., 1983. The stability of amphibole in andesite and basalt at high pressures. Am. Mineral. 68, 307–314.
Allen, R.W., Berry, C., Henstock, T.J., Collier, J.S., Dondin, F.J.-Y., Rietbrock, A., Latchman, J.L., Robertson, R.E.A., 2018. 30 years in the life of an active submarine volcano: a time-lapse bathymetry study of the Kick-'em-Jenny Volcano, Lesser Antilles. Geochem. Geophys. Geosyst. 19, 715–731.
Arculus, R.J., Delong, S.E., Kay, R.W., Brooks, C., Sun, S.S., 1977. The alkalic rock suite of Bogoslof Island, Eastern Aleutian Arc, Alaska. J. Geol. 85 (2), 177–186.
Arculus, R.J., Johnson, R.W., Chappell, B.W., McKee, C.O., Sakai, H., 1983. Ophiolite-contaminated andesites, trachybasalts, and cognate inclusions of Mount Lamington, Papua New Guinea: anhydrite-amphibole-bearing lavas and the 1951 cumulodome. J. Volcanol. Geotherm. Res. 18 (1–4), 215–247.
Barclay, J., Carmichael, I.S.E., 2004. A hornblende basalt from Western Mexico: water-saturated phase relations constrain a pressure-temperature window of eruptibility. J. Petrol. 45 (3), 485–506.
Blundy, J., Cashman, K., 2005. Rapid decompression-driven crystallization recorded by melt inclusions from Mount St. Helens volcano. Geology 33 (10), 793–796.
Blundy, J., Cashman, K., 2008. Petrologic reconstruction of magmatic system variables and processes. Rev. Mineral. Geochem. 69, 179–239.
Blundy, J., Cashman, K., Humphreys, M., 2006. Magma heating by decompression-driven crystallization beneath andesite volcanoes. Nature 443, 76–80.
Blundy, J., Cashman, K.V., Rust, A., Witham, F., 2010. A case for CO2-rich arc magmas. Earth Planet. Sci. Lett. 290 (3–4), 289–301.
Bouvier, A.-S., Metrich, N., Deloule, E., 2008. Slab-derived fluids in the magma sources of St. Vincent (Lesser Antilles Arc): volatile and light element imprints. J. Petrol. 49 (8), 1427–1448.
Brey, G.P., Kohler, T., 1990. Geothermobarometry in four-phase lherzolites II. New thermobarometers, and practical assessment of existing thermobarometers. J. Petrol. 31, 1353–1378.
Bucholz, C.E., Gaetani, G.A., Behn, M.D., Shimizu, N., 2013. Post-entrapment modification of volatiles and oxygen fugacity in olivine-hosted melt inclusions. Earth Planet. Sci. Lett. 374, 145–155.
Camejo, M., Robertson, R.E.A., 2013. Estimating Volcanic Risk in the Lesser Antilles. The University of the West Indies, St. Augustine.
Camejo-Harry, M., Melekhova, E., Blundy, J., Attridge, W., Robertson, R., Christopher, T., 2018. Magma evolution beneath Bequia, Lesser Antilles, deduced from petrology of lavas and plutonic xenoliths. Contrib. Mineral. Petrol. 173 (77).
Carey, S., Bell, K.L.C., Ballard, R.D., Roman, C., Dondin, F., Connally, P., Blake, R., Wishner, K., Phillips, T., 2014. Fluid/gas venting and biological communities at Kick 'em Jenny submarine volcano, Grenada (West Indies). Oceanography 27 (1), 38–41.
Caricchi, L., Sheldrake, T.E., Blundy, J., 2018. Modulation of magmatic processes by CO2 flushing. Earth Planet. Sci. Lett. 491, 160–171.
Carmichael, I.S.E., 2002. The andesite aqueduct: perspectives on the evolution of intermediate magmatism in west-central (105–99°W) Mexico. Contrib. Mineral. Petrol. 143 (6), 641–663.
Cashman, K.V., Sparks, R.S.J., Blundy, J.D., 2017. Vertically extensive and unstable magmatic systems: a unified view of igneous processes. Science 355, eaag3055.
Christeson, G.L., Mann, P., Escalona, A., Aitken, T.J., 2008. Crustal structure of the Caribbean–northeastern South America arc-continent collision zone. J. Geophys. Res. 113, B08104.
Christopher, T.E., Blundy, J., Cashman, K., Cole, P., Edmonds, M., Smith, P.J., Sparks, R.S.J., Stinton, A., 2015. Crustal-scale degassing due to magma system destabilization and magma-gas decoupling at Soufriere Hills Volcano, Montserrat. Geochem. Geophys. Geosyst. 16, 2797–2811.
Christopher, T.E., Constantinescu, R., Lindsay, J.M., Dondin, F., Robertson, R.E.A., 2016. Geochemistry of Kick 'em Jack and Kick 'em Jenny submarine volcanoes, Lesser Antilles. Cities on Volcanoes. 9 (Puerto Varas, Chile).
Cooper, K.M., 2017. What does a magma reservoir look like? The "crystal's-eye" view. Elements 13, 23–28.
Cooper, G.F., Davidson, J.P., Blundy, J.D., 2016. Plutonic xenoliths from Martinique, Lesser Antilles: evidence for open system processes and reactive melt flow in island arc crust. Contrib. Mineral. Petrol. 171 (87).
Devas, R.P., MacAdam-Sherwin, T., 1939. Manifestations of Volcanic Activity Observed July 24, 1939 From Gunton Estate House, Grenada.
Devine, J.D., Sigurdsson, H., 1995. Petrology and eruption styles of Kick 'em Jenny submarine volcano, Lesser Antilles island arc. J. Volcanol. Geotherm. Res. 69, 35–58.
Dondin, F., Lebrun, J.-F., Kelfoun, K., Fournier, N., Randrianasolo, A., 2012. Sector collapse at Kick 'em Jenny submarine volcano (Lesser Antilles): numerical simulation and landslide behaviour. Bull. Volcanol. 74, 595–607.
Dondin, F.J.-Y., Heap, M.J., Robertson, R.E.A., Dorville, J.-F.M., Carey, S., 2017. Flank instability assessment at Kick-'em-Jenny submarine volcano (Grenada, Lesser Antilles): a multidisciplinary approach using experiments and modeling. Bull. Volcanol. 79 (5).
Droop, G.T.R., 1987. A general equation for estimating Fe3+ concentrations in ferromagnesian silicates and oxides from microprobe analyses, using stoichiometric criteria. Min. Mag. 51, 431–435.
Ghiorso, M.S., Gualda, G.A.R., 2015. An H_2O-CO_2 mixed fluid saturation model compatible with rhyolite-MELTS. Contrib. Mineral. Petrol. 169, 1–30.
Grove, T.L., Elkins-Tanton, L.T., Parman, S.W., Chatterjee, N., Muntener, O., Gaetani, G.A., 2003. Fractional crystallization and mantle-melting controls on calc-alkaline differentiation trends. Contrib. Mineral. Petrol. 145 (5), 515–533.
Heath, E., Macdonald, R., Belkin, H., Hawkesworth, C.J., Sigurdsson, H., 1998. Magmagenesis at Soufriere Volcano, St Vincent, Lesser Antilles Arc. J. Petrol. 39 (10), 1721–1764.
Holland, T., Blundy, J., 1994. Non-ideal interactions in calcic amphiboles and their bearing on amphibole-plagioclase thermometry. Contrib. Mineral. Petrol. 116 (4), 433–447.
Holloway, J.R., Burnham, C.W., 1972. Melting relations of basalt with equilibrium water pressure less than total pressure. J. Petrol. 13 (1), 1–29.
Humphreys, M.C.S., Kearns, S., Blundy, J.D., 2006. SIMS investigation of electron-beam damage to hydrous, rhyolitic glasses: implications for melt inclusion analysis. Am. Mineral. 91, 667–679.
Krawczynski, M.J., Grove, T.L., Behrens, H., 2012. Amphibole stability in primitive arc magmas: effects of temperature, H2O content, and oxygen fugacity. Contrib. Mineral. Petrol. 164 (2), 317–339.
Kress, V.C., Carmichael, I.S.E., 1991. The compressibility of silicate liquids containing Fe2O3 and the effect of composition, temperature, oxygen fugacity and pressure on their redox states. Contrib. Mineral. Petrol. 108, 82–92.
Latchman, J.L., Robertson, R.E.A., Lynch, L.L., Dondin, F., Ramsingh, C., Stewart, R., Smith, P., Stinton, A., Edwards, S., Ash, C., Juman, A., Joseph, E.P., Nath, N., Juman, I., Ramsingh, H., Madoo, F., 2017. 2017/04/29 eruption of Kick-'em-Jenny submarine volcano. Report on the 2017/04/08-05/02 Kick-'em-Jenny unrest and eruption episode. The University of the West Indies, St. Augustine, Trinidad.
Le Bas, M.J., Le Maitre, R.W., Streckeisen, A., Zanettin, B., 1986. A chemical classification of volcanic rocks based on the total alkali–silica diagram. J. Petrol. 27, 745–750.
Leake, B.E., Woolley, A.R., Birch, W.D., Burke, E.A.J., Ferraris, G., Grice, J.D., Hawthorne, F.C., Kisch, H.J., Krivovichev, V.G., Schumacher, J.C., Stephenson, N.C.N., Whittaker, E.J.W., 2003. Nomenclature of amphiboles: additions and revisions to the International Mineralogical Association's 1997 recommendations. Can. Mineral. 41, 1355–1362.
Lindsay, J.M., Shepherd, J.B., 2005. Kick 'em Jenny & Île de Caille. In: Lindsay, J.M., Robertson, R.E.A., Shepherd, J.B., Ali, S. (Eds.), Volcanic Hazard Atlas of the Lesser Antilles. Seismic Research Unit, The University of the West Indies, Trinidad and Tobago, W.I., pp. 107–126.
Lindsay, J.M., Shepherd, J.B., Wilson, D., 2005. Volcanic and scientific activity at Kick 'em Jenny submarine volcano 2001–2002: implications for volcanic hazard in the Southern Grenadines, Lesser Antilles. Nat. Hazards 34, 1–24.
Lindsley, D.H., 1983. Pyroxene thermometry. Am. Mineral. 68, 477–493.
Luhr, J.F., Carmichael, I.S.E., 1985. Jorullo Volcano, Michoacán, Mexico (1759–1774): the earliest stages of fractionation in calc-alkaline magmas. Contrib. Mineral. Petrol. 90 (2–3), 142–161.
Mayer, B., Jung, S., Romer, R.L., Stracke, A., Haase, K.M., Garbe-Schonberg, C.-D., 2013. Petrogenesis of Tertiary hornblende-bearing lavas in the Rhon, Germany. J. Petrol. 54 (10), 2095–2123.
Melekhova, E., Blundy, J., Robertson, R., Humphreys, M.C.S., 2015. Experimental evidence for polybaric differentiation of primitive arc basalt beneath St. Vincent, Lesser Antilles. J. Petrol. 56 (1), 161–192.
Melekhova, E., Blundy, J., Martin, R., Arculus, R., Pichavant, M., 2017. Petrological and experimental evidence for differentiation of water-rich magmas beneath St. Kitts, Lesser Antilles. Contrib. Mineral. Petrol. 172 (98).
Melnik, O., Barmin, A.A., Sparks, R.S.J., 2005. Dynamics of magma flow inside volcanic conduits with bubble overpressure buildup and gas loss through permeable magma. J. Volcanol. Geotherm. Res. 143, 53–68.
Metrich, N., Wallace, P.J., 2008. Volatile abundances in basaltic magmas and their degassing paths tracked by melt inclusions. Rev. Mineral. Geochem. 69 (1), 363–402.
Moore, L.R., Gazel, E., Tuohy, R., Lloyd, A.S., Esposito, R., Steele-MacInnis, M., Hauri, E.H., Wallace, P.J., Plank, T., Bodnar, J., 2015. Bubbles matter: an assessment of the contribution of vapor bubbles to melt inclusion volatile budgets. Am. Mineral. 100, 806–823.
Nandedkar, R.H., Ulmer, P., Othmar, M., 2014. Fractional crystallization of primitive, hydrous arc magmas: an experimental study at 0.7 GPa. Contrib. Mineral. Petrol. 167, 1015.
Niida, K., Green, D.H., 1999. Stability and chemical composition of pargasitic amphibole in MORB pyrolite under upper mantle conditions. Contrib. Mineral. Petrol. 135 (1), 18–40.
Olsen, R., 2011. Hydrothermal Mineralization at a Submarine Island Arc Volcano, Kick 'em Jenny, Lesser Antilles Island Arc. (Master's Thesis). The University of Rhode Island.
Parkinson, I.J., Arculus, R.J., Eggins, S.M., 2003. Peridotite xenoliths from Grenada, Lesser Antilles Island Arc. Contrib. Mineral. Petrol. 146 (2), 241–262.
Passmore, E., Maclennan, J., Fitton, G., Thordarson, T., 2012. Mush disaggregation in basaltic magma chambers: evidence from the AD 1783 Laki Eruption. J. Petrol. 53 (12), 2593–2623.
Pichavant, M., Macdonald, R., 2007. Crystallization of primitive basaltic magmas at crustal pressures and genesis of the calc-alkaline igneous suite: experimental evidence from St Vincent, Lesser Antilles arc. Contrib. Mineral. Petrol. 154 (5), 535–558.

Pichavant, M., Mysen, B.O., Macdonald, R., 2002. Source and H2O content of high-MgO magmas in island arc settings: an experimental study of a primitive calc-alkaline basalt from St. Vincent, Lesser Antilles arc. Geochim. Cosmochim. Acta 66 (12), 2193–2209.

Plank, T., Kelley, K.A., Zimmer, M.M., Hauri, E.H., Wallace, P.J., 2013. Why do mafic arc magmas contain ~4 wt% water on average? Earth Planet. Sci. Lett. 364, 168–179.

Putirka, K.D., 2008. Thermometers and barometers for volcanic systems. Rev. Mineral. Geochem. 69 (1), 61–120.

Robertson, R.E.A., Latchan, J.L., Lynch, L., Dondin, F., Ash, C., Camejo, M., Christopher, T., Graham, O.M.H., Jackson, V., Joseph, E., Juman, A., Juman, I., Nath, N., Ramsingh, C., Ramsingh, H., Ryan, G., Smith, P., Stewart, R., Stinton, A., 2015. Report on the 2015 unrest activity at Kick-'em-Jenny submarine volcano, Grenada. The University of the West Indies, Seismic Research Centre, St. Augustine, Trinidad.

Rutherford, M.J., Hill, P.M., 1993. Magma ascent rates from amphibole breakdown: an experimental study applied to the 1980–1986 Mount St. Helens eruptions. J. Geophys. Res. 98 (B11), 19667–19685.

Shejwalkar, A., Coogan, L.A., 2013. Experimental calibration of the roles of temperature and composition in the Ca-in-olivine geothermometer at 0.1 MPa. Lithos 177, 54–60.

Shimizu, N., Arculus, R.J., 1975. Rare earth element concentrations in a suite of basanitoids and alkali olivine basalts from Grenada, Lesser Antilles. Contrib. Mineral. Petrol. 50 (4), 231–240.

Sigurdsson, H., Shepherd, J.B., 1974. Amphibole-bearing basalts from the submarine volcano Kick 'em-Jenny in the Lesser Antilles Island arc. Bull. Volcanol. 38, 891–910.

Sisson, T.W., Grove, T.L., 1993. Experimental investigations of the role of H2O in calc-alkaline differentiation and subduction zone magmatism. Contrib. Mineral. Petrol. 113 (2), 143–166.

Stamper, C.C., Blundy, J.D., Arculus, R.J., Melekhova, E., 2014a. Petrology of plutonic xenoliths and volcanic rocks from Grenada, Lesser Antilles. J. Petrol. 55 (7), 1353–1387.

Stamper, C.C., Melekhova, E., Blundy, J.D., Arculus, R.J., Humphreys, M.C.S., Brooker, R.A., 2014b. Oxidised phase relations of a primitive basalt from Grenada, Lesser Antilles. Contrib. Mineral. Petrol. 167.

Tatsumi, Y., Eggins, S., 1995. Subduction Zone Magmatism. Blackwell Science, Inc., Cambridge, MA (211 pp.).

Tollan, P.M.E., Bindeman, I., Blundy, J.D., 2011. Cumulate xenoliths from St. Vincent, Lesser Antilles Island Arc: a window into upper crustal differentiation of mantle-derived basalts. Contrib. Mineral. Petrol. 163 (2), 189–208.

Wade, J.A., Plank, T., Hauri, E.H., Kelley, K.A., Roggensack, K., Zimmer, M., 2008. Prediction of magmatic water contents via measurement of H2O in clinopyroxene phenocrysts. Geology 36 (10), 799–802.

Wadge, G., 1984. Comparison of volcanic production rates and subduction rates in the Lesser Antilles and Central America. Geology 12 (9), 555–558.

Zimmer, M.M., Plank, T., Hauri, E.H., Yogodzinski, G.M., Stelling, P., Larsen, J., Singer, B., Jicha, B., Mandeville, C., Nye, C.J., 2010. The role of water in generating the calc-alkaline trend: new volatile data for Aleutian magmas and a new Tholeiitic Index. J. Petrol. 51 (12), 2411–2444.